JEM

Deletion of Asxl1 results in myelodysplasia and severe developmental defects in vivo

Omar Abdel-Wahab,[1,2] Jie Gao,[5,6] Mazhar Adli,[7] Anwesha Dey,[11] Thomas Trimarchi,[5,6] Young Rock Chung,[1] Cem Kuscu,[7] Todd Hricik,[1] Delphine Ndiaye-Lobry,[5,6] Lindsay M. LaFave,[1,3] Richard Koche,[8,9,10] Alan H. Shih,[1,2] Olga A. Guryanova,[1] Eunhee Kim,[1] Sheng Li,[14] Suveg Pandey,[1] Joseph Y. Shin,[1] Leon Telis,[1] Jinfeng Liu,[12] Parva K. Bhatt,[1] Sebastien Monette,[15] Xinyang Zhao,[16] Christopher E. Mason,[14] Christopher Y. Park,[1,4] Bradley E. Bernstein,[8,9,10] Iannis Aifantis,[5,6] and Ross L. Levine[1,2,3,13]

[1]Human Oncology and Pathogenesis Program, [2]Leukemia Service, [3]Gerstner Sloan-Kettering Graduate School of Biomedical Sciences, and [4]Department of Pathology, Memorial Sloan-Kettering Cancer Center, New York, NY 10065
[5]Howard Hughes Medical Institute and [6]Department of Pathology, New York University School of Medicine, New York, NY 10016
[7]Department of Biochemistry and Molecular Genetics, University of Virginia, Charlottesville, VA 22908
[8]Broad Institute of MIT and Harvard, Cambridge, MA 02142
[9]Howard Hughes Medical Institute and [10]Department of Pathology, Massachusetts General Hospital, Harvard Medical School, Boston, MA 02114
[11]Department of Molecular Biology and [12]Department of Bioinformatics and Computational Biology, Genentech, South San Francisco, CA 94080
[13]Graduate School of Medical Sciences and [14]Department of Physiology and Biophysics, Weill Cornell Medical College, New York, NY 10065
[15]Tri-Institutional Laboratory of Comparative Pathology, Memorial Sloan-Kettering Cancer Center, Weill Cornell Medical College, and The Rockefeller University, New York, NY 10065
[16]Department of Biochemistry and Molecular Genetics, University of Alabama, Birmingham, AL 35294

CORRESPONDENCE
Ross L. Levine:
leviner@mskcc.org
OR
Iannis Aifantis:
iannis.aifantis@nyumc.org

Abbreviations used: AML, acute myeloid leukemia; ChIP, chromatin immunoprecipitation; CMP, common MP; DKO, double KO; EMH, extramedullary hematopoiesis; ES, embryonic stem; GMP, granulocyte/macrophage progenitor; GSEA, gene set enrichment analysis; Hb, hemoglobin; HSC, hematopoietic stem cell; HSPC, hematopoietic stem/progenitor cell; LT-HSC, long-term HSC; MDS, myelodysplastic syndrome; MEP, megakaryocyte/erythroid progenitor; MP, myeloid progenitor; MPN, myeloproliferative neoplasm; MPP, multipotent progenitor; polyI:polyC, polyinosinic-polycytidylic acid; qRT-PCR, quantitative real-time PCR; TSS, transcription start site.

Somatic *Addition of Sex Combs Like 1* (*ASXL1*) mutations occur in 10–30% of patients with myeloid malignancies, most commonly in myelodysplastic syndromes (MDSs), and are associated with adverse outcome. Germline *ASXL1* mutations occur in patients with Bohring–Opitz syndrome. Here, we show that constitutive loss of *Asxl1* results in developmental abnormalities, including anophthalmia, microcephaly, cleft palates, and mandibular malformations. In contrast, hematopoietic-specific deletion of *Asxl1* results in progressive, multilineage cytopenias and dysplasia in the context of increased numbers of hematopoietic stem/progenitor cells, characteristic features of human MDS. Serial transplantation of *Asxl1*-null hematopoietic cells results in a lethal myeloid disorder at a shorter latency than primary *Asxl1* knockout (KO) mice. *Asxl1* deletion reduces hematopoietic stem cell self-renewal, which is restored by concomitant deletion of *Tet2*, a gene commonly co-mutated with *ASXL1* in MDS patients. Moreover, compound *Asxl1/Tet2* deletion results in an MDS phenotype with hastened death compared with single-gene KO mice. *Asxl1* loss results in a global reduction of H3K27 trimethylation and dysregulated expression of known regulators of hematopoiesis. RNA-Seq/ChIP-Seq analyses of Asxl1 in hematopoietic cells identify a subset of differentially expressed genes as direct targets of Asxl1. These findings underscore the importance of Asxl1 in Polycomb group function, development, and hematopoiesis.

Candidate gene and genome-wide discovery studies have identified a set of novel disease alleles in patients with myelodysplastic syndromes (MDSs), acute myeloid leukemia (AML), and myeloproliferative neoplasms (MPNs). These

include somatic mutations in genes with a known or putative role in the epigenetic regulation of gene expression (Shih et al., 2012). *Addition of*

O. Abdel-Wahab, J. Gao, and M. Adli contributed equally to this paper.

Supplemental Material can be found at:
http://jem.rupress.org/content/suppl/2013/11/08/jem.20131141.DC1.html

JEM

Sex Combs Like 1 (*ASXL1*) is a Polycomb-associated protein that has been shown to be an essential cofactor for the nuclear deubiquitinase BAP1 (Dey et al., 2012), as well as a critical mediator of the function of the Polycomb repressive complex 2 (PRC2; Abdel-Wahab et al., 2012). Recurrent somatic loss-of-function mutations and deletions in *ASXL1* are observed in MDS, MPN, and AML patients (Gelsi-Boyer et al., 2009). *ASXL1* mutations are most common in MDS patients (Bejar et al., 2011, 2012; Thol et al., 2011; Sanada and Ogawa, 2012), including in 15–20% of MDS patients and in 40–60% in patients with MDS/MPN overlap syndromes (Gelsi-Boyer et al., 2009; Boultwood et al., 2010; Jankowska et al., 2011). *ASXL1* mutations are associated with adverse overall survival in MDS, chronic myelomonocytic leukemia, AML, and MPN (Bejar et al., 2011, 2012; Metzeler et al., 2011; Patel et al., 2012; Itzykson et al., 2013; Vannucchi et al., 2013), highlighting the relevance of *ASXL1* mutations to myeloid transformation and clinical outcome.

More recently, de novo constitutive *ASXL1* mutations were identified in children with the developmental disorder Bohring-Opitz syndrome (Hoischen et al., 2011; Magini et al., 2012). Although these genetic data strongly implicate *ASXL1* mutations in myeloid malignancies and in developmental defects, our understanding of the role of Asxl1 in steady-state hematopoiesis, hematopoietic stem/progenitor function, and myeloid malignancies has been limited by the lack of a mouse model for conditional and tissue-specific deletion of Asxl1. Fisher et al. (2010a,b) investigated the role of Asxl1 in hematopoiesis through the creation and analysis of a model of constitutive *Asxl1* deletion with targeted insertion of a neo cassette into the *Asxl1* locus. Disruption of *Asxl1* expression in this manner resulted in partial perinatal lethality. Analysis of the remaining aged (beyond 15 wk of age) *Asxl1* mutant mice revealed impairment of B and T cell lymphopoiesis and myeloid differentiation. However, constitutive *Asxl1* loss did not alter long-term reconstitution in competitive repopulation studies using *Asxl1*-null fetal liver cells (Fisher et al., 2010a,b). These results suggested that *Asxl1* has an important role in normal hematopoiesis; however, the effects of somatic loss of *Asxl1* in hematopoietic cells were not evaluated. Here we investigate the effects of *Asxl1* loss in a time- and tissue-dependent manner through the generation of a mouse model for conditional deletion of *Asxl1*. We also characterized the effect of *Asxl1* loss on transcriptional output and gene regulation using epigenomic and transcriptomic analysis of hematopoietic stem/progenitor cells (HSPCs) from WT and *Asxl1*-deficient mice.

RESULTS

Development of a conditional *Asxl1* KO allele

To delineate the role of *Asxl1* in development and in hematopoiesis, we generated a conditional allele targeting *Asxl1* in vivo (Fig. 1, A and B). We used embryonic stem (ES) cell targeting to insert two LoxP sites flanking exons 5–10 of *Asxl1*, as well as an Frt-flanked neomycin selection cassette in the upstream intron (Fig. 1, A and B). The generated mice (*Asxl1*$^{fl/fl}$) were initially crossed to a germline Flp-deleter mouse line to eliminate the neomycin cassette and then subsequently crossed to germline *EIIa-cre* mice, IFN-α–inducible *Mx1-cre*, and hematopoietic-specific *Vav-cre* (all as described below). Asxl1 protein expression was not detectable in hematopoietic tissue from *Vav-cre* and *Mx1-cre* mice (Fig. 2 B), consistent with generation of a KO allele.

Germline *Asx1* loss results in embryonic lethality and craniofacial abnormalities

We characterized the effects of constitutive deletion of *Asxl1* by crossing mice bearing floxed *Asxl1* alleles with germline *EIIa*-cre mice. The Asxl1 floxed allele was completely recombined in *EIIa-cre Asxl1*$^{fl/fl}$ mice (not depicted). We observed 100% embryonic lethality in mice with germline complete deletion of *Asxl1* (*Asxl1*$^{\Delta/\Delta}$), whereas mice with heterozygous germline deletion of Asxl1 (*Asxl1*$^{+/\Delta}$) were born at expected Mendelian ratios (Fig. 1 C). *Asxl1*$^{\Delta/\Delta}$ mice were no longer viable by embryonic day (E) 19.5 and were characterized by microphthalmia/anophthalmia (seen in 12/12 of homozygous *Asxl1*-null embryos examined; Fig. 1, D and E), frequent cleft palates (seen in 5/12 of homozygous *Asxl1*-null embryos examined; Fig. 1 E), and multiple skeletal abnormalities (mandibular hypoplasia, loss of hyoid bone formation, and posterior homeotic transformations; seen in 4/12 of homozygous *Asxl1*-null embryos examined; Fig. 1 F). *Asxl1*$^{+/\Delta}$ were viable but exhibited craniofacial dysmorphism in 35% (14/40) of adult *Asxl1*$^{+/\Delta}$ mice examined (Fig. 1 G). Immunophenotypic analysis of HSPCs and erythroid precursor cells in fetal liver from control, *Asxl1*$^{+/\Delta}$, and *Asxl1*$^{\Delta/\Delta}$ mice at E14.5 did not reveal differences among the genotypes (Fig. 1, H and I).

Hematopoietic–specific deletion of *Asxl1* results in MDS

Asxl1 is expressed throughout the adult hematopoietic compartment (Fig. 2 A). To elucidate the effects of *Asxl1* loss on postnatal hematopoiesis, *Asxl1*$^{fl/fl}$ mice were crossed to *Vav-cre* and IFN-α–inducible *Mx1-cre* transgenic mice for conditional deletion of *Asxl1* in the hematopoietic compartment (termed as *Asxl1* KO hereafter). In both cases, Asxl1 protein expression was not detectable in hematopoietic tissue (Fig. 2 B). Mice with hematopoietic-specific deletion of *Asxl1* (*Vav-cre Asxl1*$^{fl/fl}$) developed progressive BM and splenic hypocellularity relative to littermate controls (Cre⁻ *Asxl1*$^{fl/fl}$) beginning at 6 wk of age and likewise evident at 24 wk of age (n = 6–10 mice per genotype at each time point examined; Fig. 2 C). *Asxl1* KO mice, but not littermate controls, developed progressive leukopenia (Fig. 2 D) and anemia (Fig. 2 E) that was most apparent at 6–12 mo of age. Although the hemoglobin (Hb) in *Asxl1* KO mice was within normal limits (median of 13.4 g/dl, range 12.9–14.8 g/dl) in mice <6 mo of age, between 6 and 12 mo the Hb was a median of 8 g/dl (range 1.94–13.9 g/dl) in KO mice relative to a median of 11.4 g/dl in age-matched littermate control mice (range 7.17–14.2 g/dl; n = 6–12 mice with each genotype at each time point examined; Fig. 2 E). Similarly, the WBC count was within normal limits in *Asxl1*-null mice at <6 mo of age (median of 7.64×10^9 cells/µl, range $4.66–9.6 \times 10^9$ cells/µl), the WBC count fell to a median of 2.51×10^9 cells/µl (range $0.88–5.18 \times 10^9$ cells/µl)

Conditional deletion of Asxl1 results in MDS | Abdel-Wahab et al.
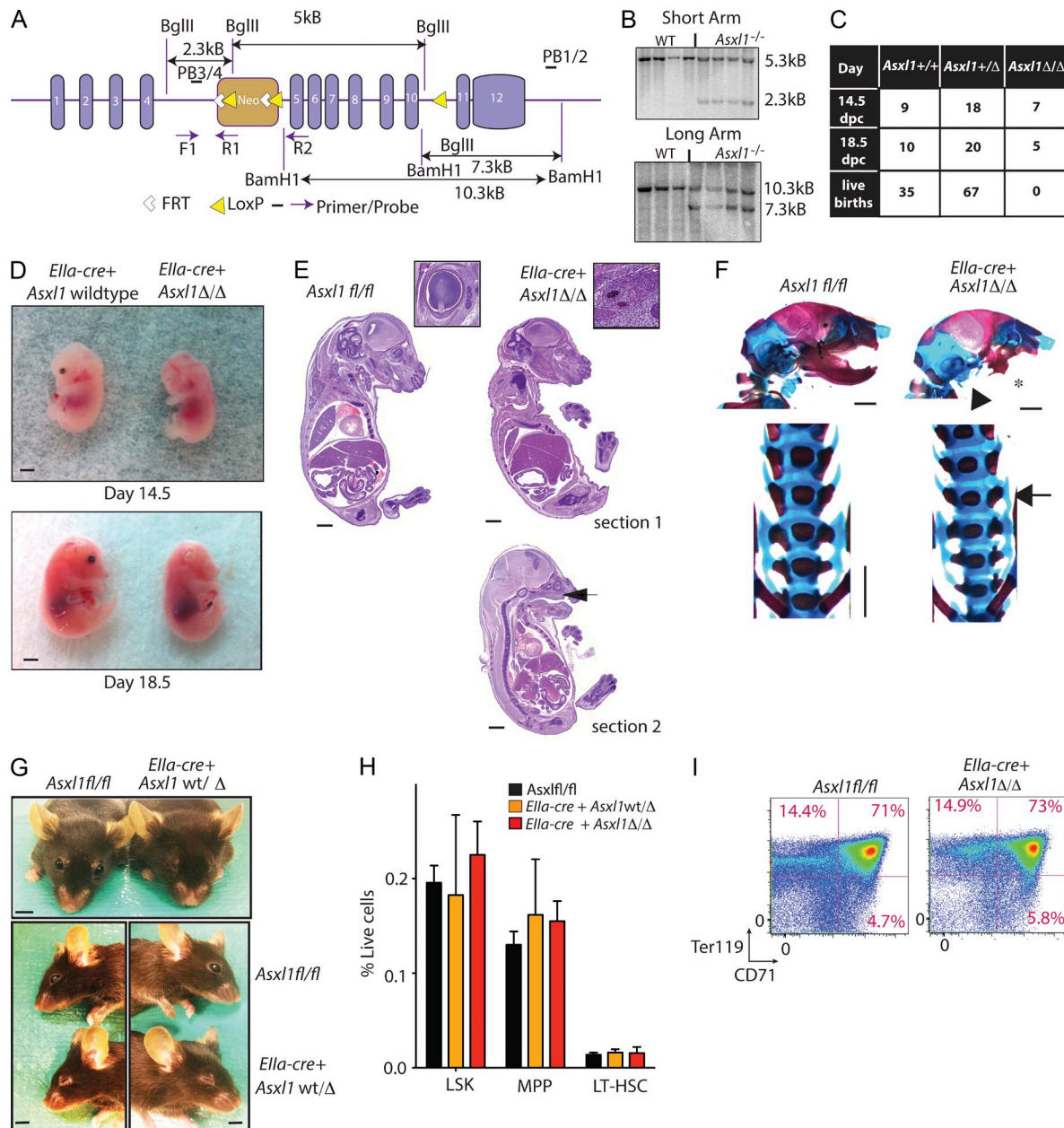
Figure 1.   Generation of a conditional *Asxl1* allele and characterization of mice with constitutive *Asxl1* loss. (A) Schematic depiction of the targeted *Asxl1* allele. Exons 5–10 are targeted and flanked by *LoxP* sites upon Frt-mediated deletion of the Neo cassette. (B) Verification of correct homologous recombination of Asxl1-targeted allele using Southern blots on targeted ES cells. (C) Enumeration of offspring derived from mating *EIIa-cre Asxl1$^{+/\Delta}$* parents. (D and E) Gross pathology (D) and tissue sections (E) of *Asxl1$^{\Delta/\Delta}$* mice at 14.5 and 18.5 d postcoitus (dpc). (F) Analysis of skeletal preparations from germline *Asxl1*-null mice surviving to E20.5 including hypoplastic mandibles (asterisk), lack of hyoid bone (arrowhead), and lower lumbar/sacral posterior homeotic transformations (arrow). (G) Gross phenotype of *EIIa-cre Asxl1$^{+/\Delta}$* and littermate control mice on bilateral microphthalmia. Bars: (D) 2 mm; (E and F [top]) 1 mm; (F, bottom) 2.5 mm; (G) 0.5 cm. (H) Immunophenotyping of fetal liver at 14.5 dpc on relative frequency of LSK cells, MPP cells (LSK, CD48$^+$, CD150$^-$ cells), and LT-HSCs (LSK, CD48$^-$, CD150$^+$ cells) between mice with germline loss of 0, 1, or 2 copies of *Asxl1*. FACS analysis was performed with three to five independent fetal liver samples per genotype. (I) FACS analysis of fetal liver at 14.5 dpc reveals relative frequency of CD71$^+$ single-positive, CD71/Ter119 double-positive, or Ter119 single-positive cells with constitutive loss of *Asxl1*. Antibody stainings are as indicated, and cells were gated on live cells in the parent gate. Error bars represent ±SD.

in *Asxl1* KO mice between the ages of 6 and 12 mo compared with age–matched littermate *Asxl1* WT mice (median WBC count of 4.51×10^9 cells/µl, range $2.62–13.8 \times 10^9$ cells/µl; Fig. 2 D). The leukopenia was predominantly caused by decrements in B220$^+$ mature B cells, CD11b$^+$ Gr1$^+$ neutrophils, and CD11b$^+$ Gr1$^-$ monocytes as indicated by flow cytometric and morphological analysis of peripheral blood (Fig. 2, F and G). The age–dependent anemia observed in
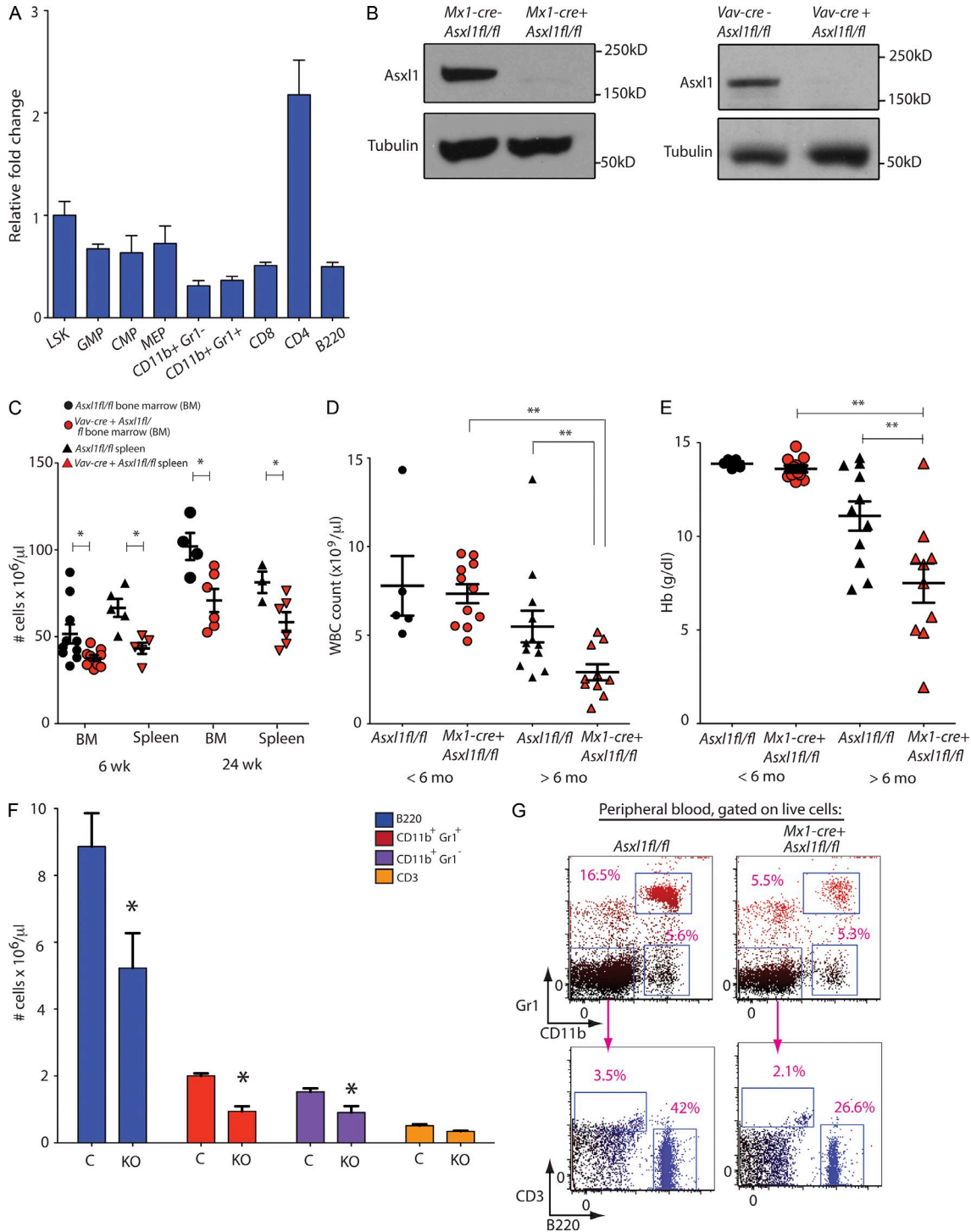
Figure 2. Conditional deletion of *Asxl1* results in age-dependent leukopenia and anemia. (A) qRT-PCR showing relative expression level of *Asxl1* in purified progenitor and mature mouse hematopoietic stem and progenitor subsets. (B) Verification of *Mx1-cre*– and *Vav-cre*–mediated deletion of *Asxl1* at the level of protein expression in Western blot of splenocytes. (C) Enumeration of nucleated cells in bilateral femurs and tibiae or whole spleens of control (*Asxl1^fl/fl^*) and *Asxl1* hematopoietic-specific KO mice (*Vav-cre Asxl1^fl/fl^*) at 6 as well as 24 wk of age (n = 6–10 mice per genotype at each time point examined). (D and E) Enumeration of peripheral WBCs (D) and Hb (E) with postnatal deletion of *Asxl1* (performed using *Mx1-cre Asxl1^fl/fl^* mice or Cre⁻ *Asxl1^fl/fl^* controls). Counts in aged *Asxl1* KO mice are compared with age-matched controls as well as younger KO and control mice (n = 6–12 mice per genotype at each time point examined). (F and G) Flow cytometric enumeration of B220⁺, CD11b⁺/Gr1⁺, CD3⁺, and CD11b⁺/Gr1⁻ cells in the peripheral blood of >6-mo-old *Mx1-cre Asxl1^fl/fl^* (KO) and *Asxl1^fl/fl^* (C) mice (n = 5 mice per genotype were used for FACS analysis of peripheral blood). The right panel reveals peripheral blood FACS analysis. Antibody stainings are as indicated, and cells were gated on live cells in the parent gate. (A and C–F) Error bars represent ±SD (A and F); mean ± SEM is shown (C–E); *, P < 0.05; **, P < 0.001 (Mann–Whitney *U* test).
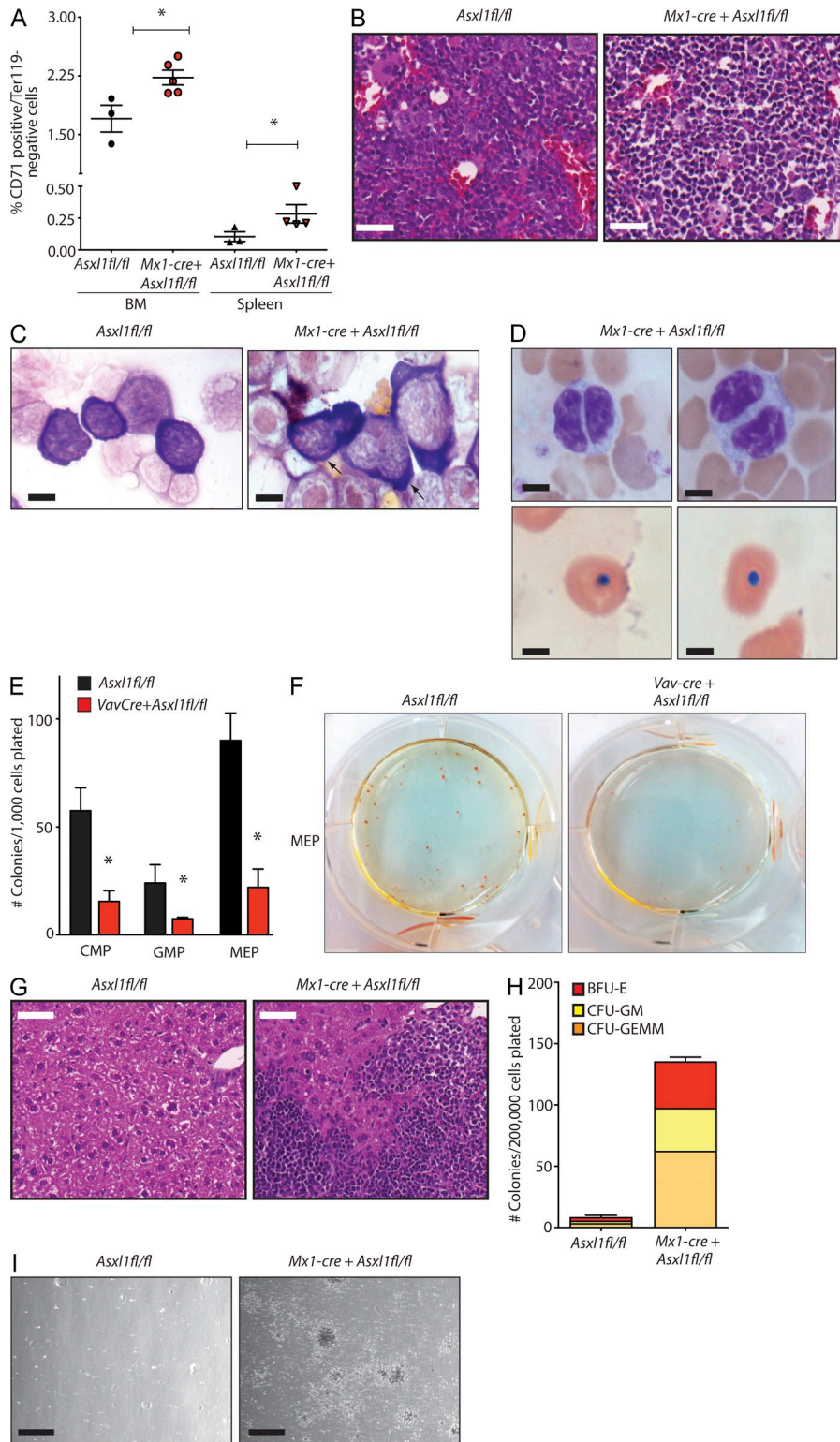
Figure 3. Deletion of *Asxl1* results in myeloid and erythroid dysplasia and impaired progenitor differentiation consistent with myelodysplasia. (A) Relative frequency of CD71$^+$/Ter119$^-$ erythroid precursors in BM and spleen of 6.5-mo-old *Mx1-cre Asxl1$^{fl/fl}$* (KO) and Cre$^-$ *Asxl1$^{fl/fl}$* control mice (expressed as percentage of live cells; n = 3–5 mice per genotype in each tissue type examined by FACS analysis). (B) Histological (H&E) analysis of *Mx1-cre Asxl1$^{fl/fl}$* and Cre$^-$ *Asxl1$^{fl/fl}$* control BM from 6-mo-old littermate mice. (C) BM cytospins (Wright-Giemsa) from the same mice (arrows indicate erythroid precursors with prominent irregular nuclear contours). (D) Representative morphology of peripheral blood myeloid cells (top) and nucleated RBCs (bottom) in KO mice (Wright-Giemsa stain). (E) Number of colonies formed 7 d after plating of 1,000 CMP, GMP, or MEP cells into methylcellulose from 6-wk-old *Vav-cre Asxl1$^{fl/fl}$* and littermate control (Cre$^-$ *Asxl1$^{fl/fl}$* control) mice. The experiment was performed in biological duplicate. (F) Photograph of methylcellulose colony plate 7 d after plating of MEP cells from 6-wk-old KO and control mice. (G) Histological analysis by H&E staining of liver from 72-wk-old *Mx1-cre Asxl1$^{fl/fl}$* mice and littermates. (H) Number of colonies formed 7 d after plating of 200,000 nucleated cells harvested from the liver of 72-wk-old *Mx1-cre Asxl1$^{fl/fl}$* or littermate control mice in methylcellulose containing rmIL-3, rm-SCF, rh-IL6, rh-EPO (liver cells from n = 5 mice per genotype plated in methylcellulose). (I) Photomicrograph of colonies grown from cells taken from the liver and plated in methylcellulose is shown on right. Bars: (B) 50 µm; (C) 10 µm; (D) 5 µm; (G) 100 µm; (I) 200 µm. Error bars represent ±SD; *, P < 0.05 (Mann–Whitney *U* test).

Asxl1 KO mice was accompanied by an increase (median 1.4- to 2-fold) in CD71$^+$/Ter119$^-$ erythroid precursor cells in both the BM and spleen, consistent with impaired erythroid differentiation (Fig. 3 A).

Pathological analysis of *Asxl1* KO hematopoietic tissues at 6 mo of age revealed morphological dysplasia of circulating myeloid cells (Fig. 3 D), frequent circulating nucleated red cells (Fig. 3 D), hypocellular marrow (Fig. 3 B), and dysplasia of erythroid precursors (Fig. 3 C). Previous characterization of HSPCs from patients with MDS (Sawada et al., 1993, 1995) and mouse models of MDS (such as the *NUP98-HOXD13* transgenic mouse model [Choi et al., 2008]) have
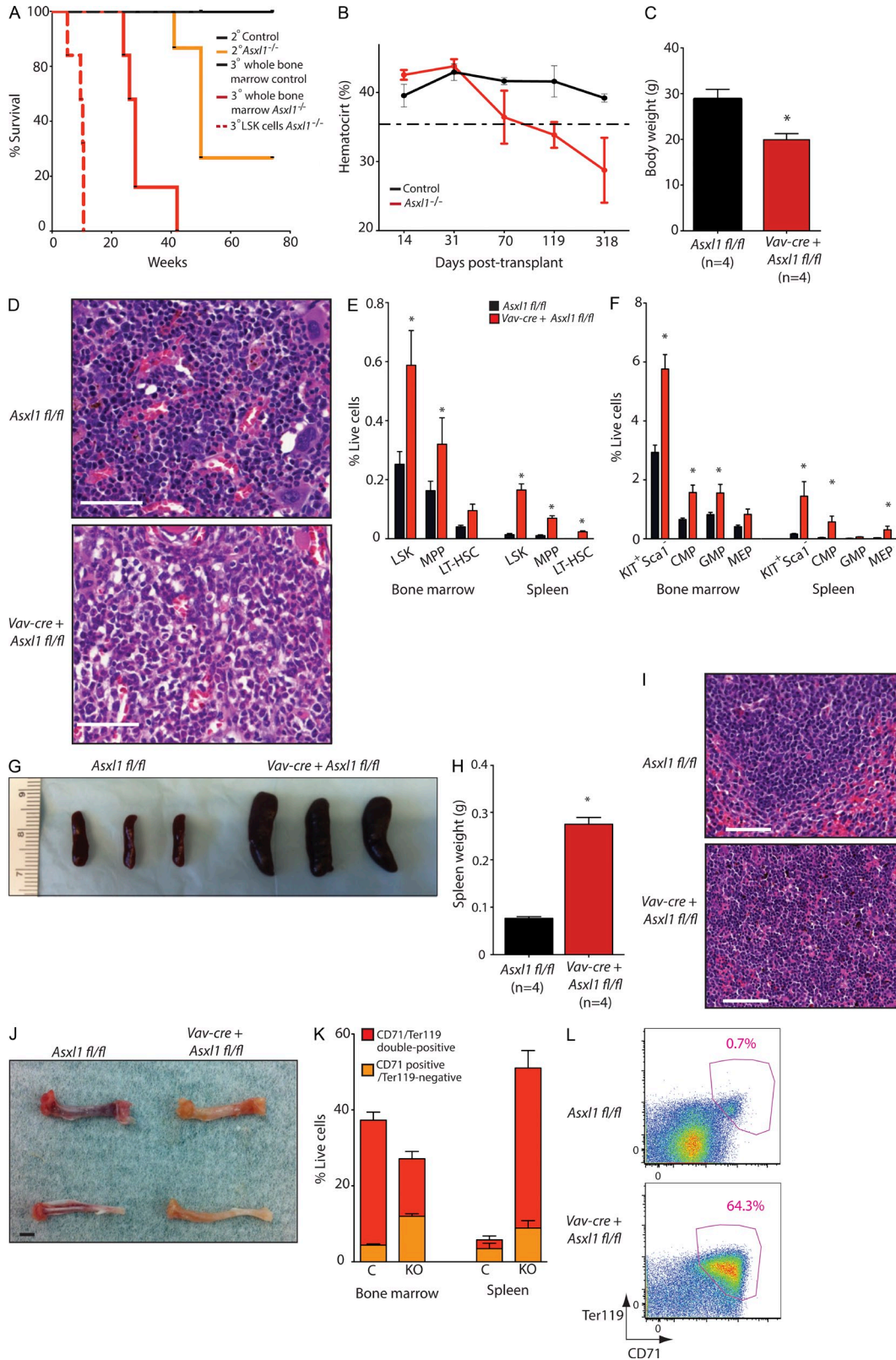
Figure 4.   Serial noncompetitive transplantation of *Asxl1*–null cells results in lethal myelodysplastic disorder. (A) Kaplan-Meier survival curve of recipient mice transplanted with 70-wk-old *Vav-cre Asxl1^fl/fl* or Cre⁻ *Asxl1^fl/fl* littermate control whole BM after secondary and tertiary transplantation. Also shown is the survival of mice transplanted with purified LSK cells in tertiary transplantation (tertiary transplant of *Asxl1^fl/fl* control LSK cells is not shown; no recipient mice from this group died by 40 wk [*n* = 5]). Cre⁻ *Asxl1^fl/fl* littermate controls were similarly transplanted in parallel in each

2646

Conditional deletion of Asxl1 results in MDS | Abdel-Wahab et al.

identified an impairment of sorted hematopoietic progenitors to form colonies ex vivo in methylcellulose containing myeloid and erythroid cytokines. Consistent with these prior observations and the impairment in mature myeloid and erythroid differentiation seen in *Asxl1*-deficient mice, in vitro analysis of sorted myeloid progenitor (MP) cells from 6-wk-old *Asxl1* KO and control mice revealed a clear decrease in colony output of sorted common MPs (CMPs), granulocyte/macrophage progenitors (GMPs), and megakaryocyte/erythroid progenitors (MEPs) in KO versus control mice (Fig. 3, E and F).

Consistent with the age-dependent development of impaired myeloid and erythroid output in *Asxl1* KO mice compared with age-matched littermate controls, *Asxl1* KO (*Mx1-cre Asxl1^{fl/fl}*) mice were found to have infiltration of liver with hematopoietic cells consistent with extramedullary hematopoiesis (EMH) with *Asxl1* deletion (Fig. 3 G). To ascertain whether this hematopoietic infiltrate represented inflammatory infiltration of hematopoietic cells versus EMH, we plated 200,000 cells harvested from the liver of *Asxl1* KO mice and littermate controls in methylcellulose semisolid media containing myeloid-erythroid cytokines (rmIL-3, rmSCF, rh-EPO, and rh-IL6). Colonies plated with cells derived from *Asxl1* KO mice alone yielded abundant colonies (Fig. 3, H and I), demonstrating EMH.

Cell-autonomous effects of *Asxl1* loss

Transplantation of whole BM from Asxl1 KO (*Vav-cre Asxl1^{fl/fl}*) mice into lethally irradiated recipients resulted in a penetrant, lethal hematopoietic disorder (Fig. 4 A), indicating that the phenotype induced by *Asxl1* loss was cell autonomous. For example, transplantation of whole BM from 70-wk-old primary *Asxl1* KO mice into lethally irradiated recipients resulted in the death of recipient mice at a median of 50 wk after transplant (range 41–74 wk), whereas no mice transplanted with *Asxl1* WT BM died during this period of observation. Furthermore, serial transplantation into tertiary recipients resulted in shorter latency of disease, with mice

dying 24–42 wk after transplant (median of 28 wk). Transplantation of purified lineage⁻ Sca-1⁺ c-KIT⁺ (LSK) cells from the BM of secondary recipients led to a lethal myeloid disease in all tertiary transplant recipients with more rapid onset (median of 10.3 wk, range 5.1–10.6 wk) than transplantation of unfractionated BM cells from the same secondary recipients (Fig. 4 A). Disease in transplanted mice was characterized by progressive anemia and cachexia (Fig. 4, B and C), BM hypocellularity (Fig. 4 D), and an increase in the relative frequency of HSPCs in both the BM and the spleen (Fig. 4, E and F). This was accompanied by splenomegaly caused by EMH and effacement of splenic architecture (Fig. 4, G–I). Anemia in the KO-transplanted recipient mice was evident even with gross inspection of bones (Fig. 4 J). As in primary *Asxl1* KO mice, this anemia occurred despite an increase in erythroid precursors in both the BM and spleen (Fig. 4, K and L), consistent with a block in erythroid differentiation with *Asxl1* loss. This block in erythroid differentiation was characterized by a significant increase in CD71/Ter119 double-positive erythroid precursors in the spleen (Fig. 4 L).

Impaired self-renewal of Asxl1-deficient cells is rescued by concomitant Tet2 loss

We next assessed the effects of *Asxl1* loss on hematopoietic stem cell (HSC) frequency and function. We observed an increase in the absolute number of immunophenotypically defined HSPCs in Asxl1 KO (*Vav-cre Asxl1^{fl/fl}*) mice at 6 wk of age, including long-term HSCs (LT-HSC; CD150⁺ CD48⁻ Lin⁻ Sca-1⁺ c-Kit⁺; Fig. 5, A and B; quantified as the total number of live cells per femur). Although the number of immunophenotypic stem/progenitor cells was increased, we observed a decrease in serial plating in vitro in *Asxl1* KO cells (Fig. 6 A), suggesting a potential defect in self-renewal. To assess the effects of *Asxl1* deletion in vivo, 500,000 whole BM nucleated cells from 6-wk-old CD45.2 *Vav-cre Asxl1^{fl/fl}* mice or *Asxl1^{fl/fl}* littermate controls were transplanted in competition with an equal number of 6-wk-old CD45.1 competitor BM cells into lethally irradiated CD45.1 recipient mice (Fig. 5 C).

experiment. Four to six recipient mice were transplanted in each experiment. (B) Hematocrit over time of secondary recipient mice transplanted with *Asxl1*-null or littermate control whole BM in a noncompetitive manner. The dashed line represents the lower limit of normal hematocrit for C57BL/6 mice (*n* = 4–6 mice per genotype at each time point). (C) Body weight of secondarily transplanted mice at 50 wk after transplantation (*n* = 4 mice per genotype). (D) BM histopathology of secondary recipient mice transplanted with *Asxl1*-null or littermate control whole BM at 50 wk. (E) Relative frequency of LSK cells, MPP cells (LSK⁺, CD150⁻, CD48⁺), and LT-HSCs (LSK⁺ CD150⁺ CD48⁻) in BM and spleen at 50 wk after noncompetitive secondary transplantation. Frequencies are expressed as frequency of live cells (*n* = 4 mice per genotype examined for FACS experiments). (F) Relative frequency of MP (lineage⁻ c-Kit⁺ Sca-1⁻), CMP (lineage⁻, c-Kit⁺, Sca-1⁻, FcγR⁻, CD34⁺), GMP (lineage⁻ c-Kit⁺ Sca-1⁻, FcγR⁺ CD34⁺), and MEP (lineage⁻ c-Kit⁺ Sca-1⁻ FcγR⁻ CD34⁻) cells at 50 wk after noncompetitive secondary transplantation. Frequencies are expressed as a frequency of live cells. (G) Photographs of spleens from secondary recipient mice transplanted with *Vav-cre Asxl1^{fl/fl}* or Cre⁻ *Asxl1^{fl/fl}* littermate control whole BM 50 wk after lethal irradiation. (H) Weight of the same spleens as shown in G (*n* = 4 mice per genotype). (I) Histopathology of spleens from secondary recipient mice transplanted with *Asxl1*-null or WT littermate control whole BM 50 wk after noncompetitive secondary transplantation revealing loss of normal splenic architecture. (J) Photographs of representative femur (top) and tibia (bottom) from secondary recipient mice transplanted with *Vav-cre Asxl1^{fl/fl}* or Cre⁻ *Asxl1^{fl/fl}* littermate control whole BM 50 wk after noncompetitive secondary transplantation. Bars: (D and I) 50 μm; (J) 2 mm. (K) Relative quantification of CD71⁺/Ter119⁻ and CD71/Ter119 double-positive cells from BM and spleen of secondary recipient mice transplanted with *Vav-cre Asxl1^{fl/fl}* or Cre⁻ *Asxl1^{fl/fl}* littermate control whole BM 50 wk after noncompetitive secondary transplantation. Frequencies are expressed as a percentage of live cells (*n* = 4 mice per genotype examined by FACS analysis). (L) Representative FACS plots of data shown in K from splenocytes. Staining is as shown, and live cells were gated in parent gate. Error bars represent ±SD; *, P < 0.05 (Mann–Whitney *U* test).
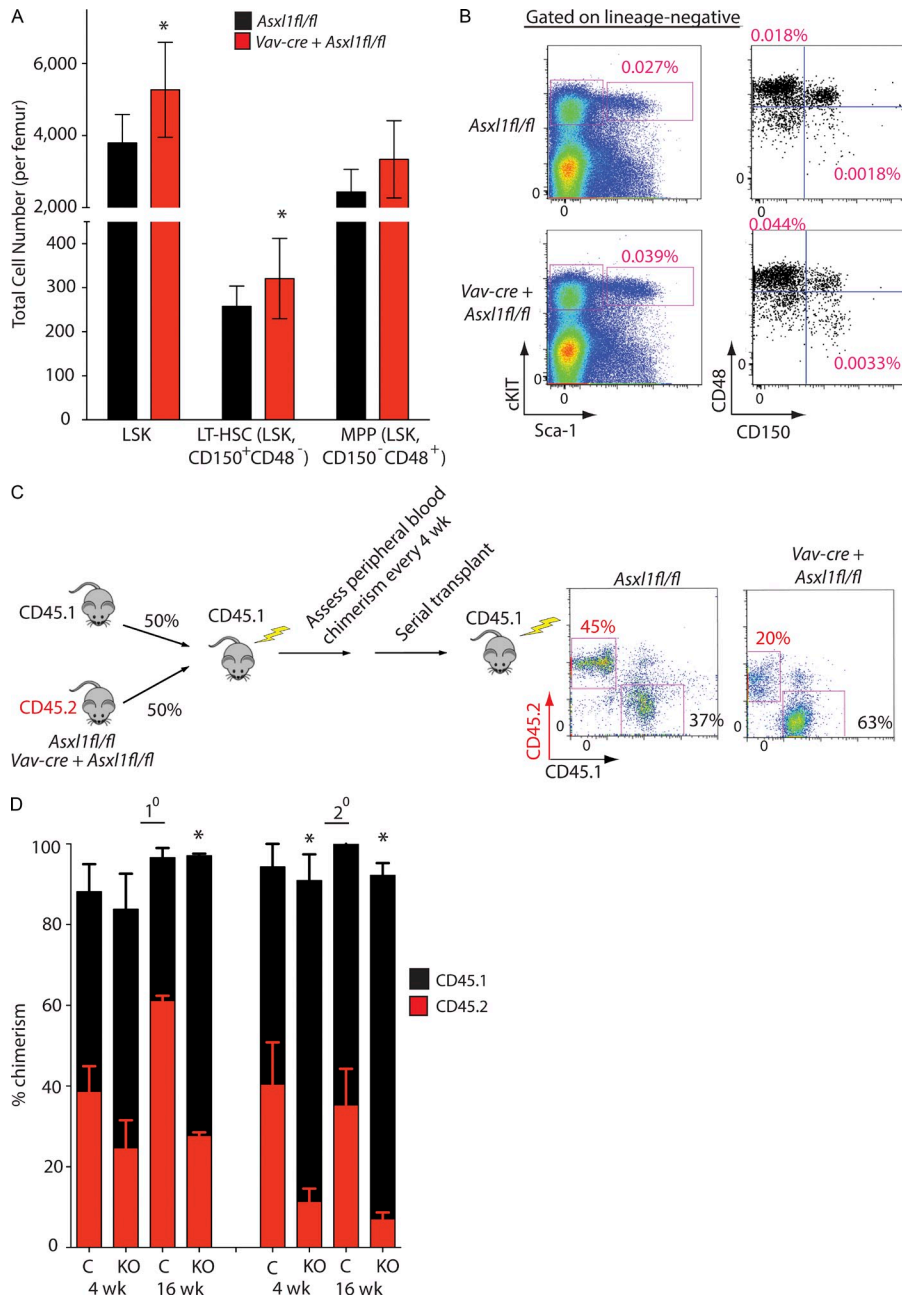
Figure 5. *Asxl1⁻/⁻* mice have increased stem/progenitor cells but impaired self-renewal. (A) Flow cytometric enumeration of BM LSK cells, LT-HSCs (LSK CD150⁺ CD48⁻), and MPP cells (LSK CD150⁻ CD48⁺) in WT (*Asxl1ᶠˡ/ᶠˡ*) and KO (*Vav-cre Asxl1ᶠˡ/ᶠˡ*) mice at 6 wk of age (*n* = 4–6 mice per genotype as indicated). Data are expressed as total number of live cells per femur. (B) Representative FACS analysis of BM stem cell populations of *Asxl1⁻/⁻* (*Vav-cre Asxl1ᶠˡ/ᶠˡ*) and WT (*Asxl1ᶠˡ/ᶠˡ*) at 6 wk. Antibody stains are as indicated and parent gate is live, lineage⁻ cells. (C) Schematic depiction of the competitive transplantation assay. *Asxl1ᶠˡ/ᶠˡ* and *Vav-cre Asxl1ᶠˡ/ᶠˡ* are positive for CD45.2, whereas WT competitor cells are positive for CD45.1. Recipient mice are also CD45.1. Representative FACS plots of the percentage of CD45.1 versus CD45.2 total chimerism in the peripheral blood of recipient animals at 16 wk after competitive transplantation is shown. (D) Percentage of CD45.1 versus CD45.2 total chimerism in the peripheral blood of recipient animals at 4 and 16 wk in primary competitive transplant and serial secondary competitive transplants are shown (*n* = 5 recipient mice for each genotype; C, control; KO, *Asxl1* KO). The experiment was performed in biological duplicate. Error bars represent ±SD; *, P < 0.05 (Mann–Whitney *U* test).

Chimerism was assessed based on evaluation of the ratio of CD45.1 to CD45.2 peripheral blood mononuclear cells beginning 2 wk after transplantation and then monitored on a monthly basis until 16 wk thereafter. Consistent with the in vitro data, we observed a clear reduction in self-renewal in vivo. *Asxl1* KO HSPCs had a significant disadvantage in competitive transplantation that was further accentuated with serial transplantation (Fig. 5, C and D).

After the final assessment of chimerism in the primary competitive transplantation experiments, primary recipient mice were sacrificed and a serial competitive transplantation experiment was performed by transplanting 1 million whole BM cells from primary recipient mice into lethally irradiated CD45.1 secondary recipient mice (Fig. 5 D). Serial competitive transplantation revealed an even further competitive disadvantage in *Asxl1*-deficient HSPCs (Fig. 5 D).

Given that MDS is characterized by impaired myeloid differentiation, multilineage cytopenias, and clonal dominance over time, we hypothesized that mutations that occur in concert with *ASXL1* deletion/mutation in MDS might compensate for the impaired self-renewal observed with Asxl1 loss. Previous studies have shown that mutations in *TET2* are most commonly observed with mutations in *ASXL1* in MDS (Bejar et al., 2011, 2012). We and others previously demonstrated increased hematopoietic self-renewal in Tet2-deficient mice (Ko et al., 2011; Li et al., 2011; Moran-Crusio et al.,
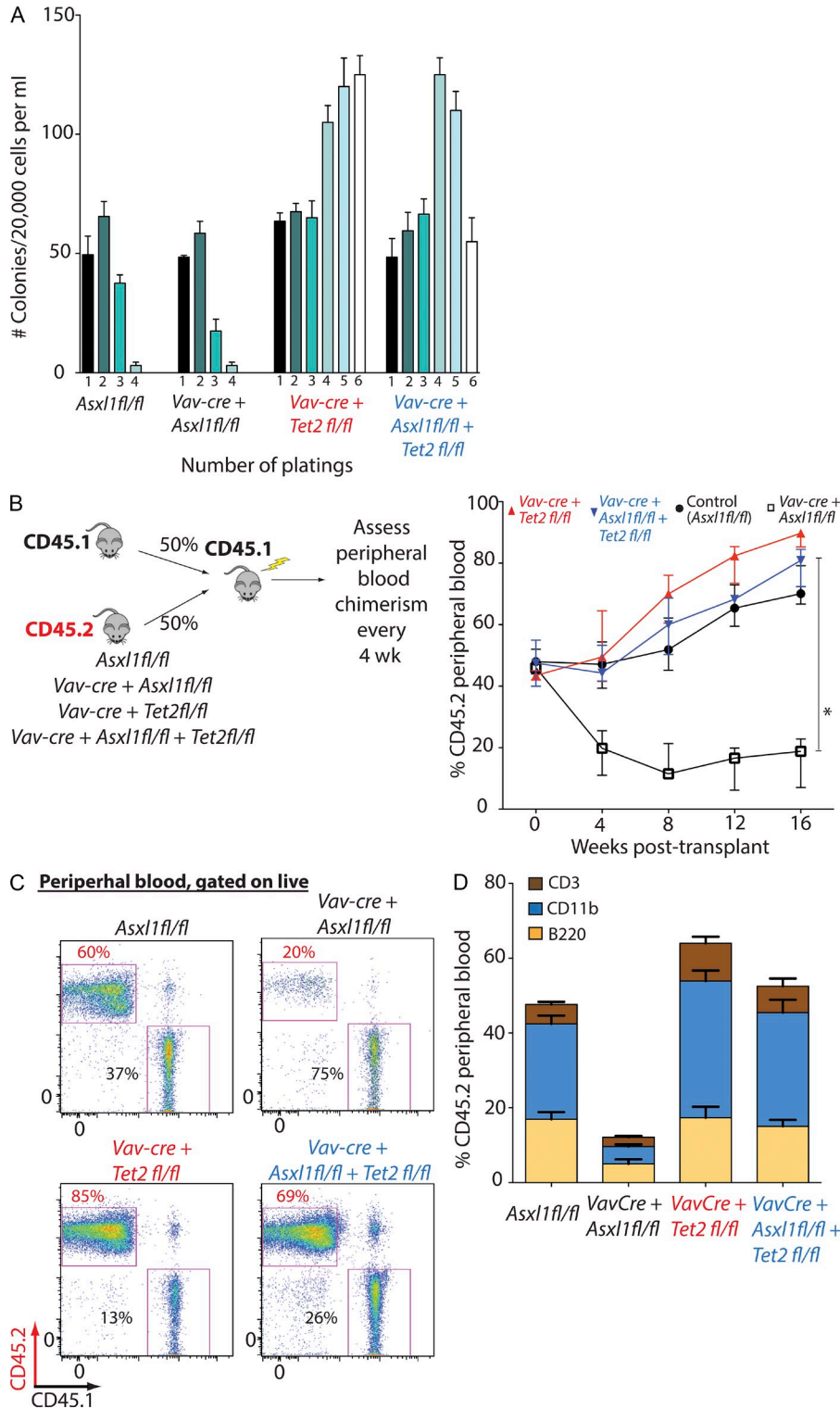
Figure 6. Combined loss of *Asxl1* and *Tet2* rescues the impaired self-renewal of *Asxl1*-deficient HSCs. (A) Enumeration of colonies and serial replating capacity of 20,000 whole BM cells from 6-wk-old littermate mice with hematopoietic-specific deletion of *Asxl1* (*Vav-cre Asxl1fl/fl*), *Tet2* (*Vav-cre Tet2fl/fl*), or both (*Vav-cre Asxl1fl/fl Tet2fl/fl*). (B) Schematic depiction of the competitive transplantation experiment. Control, *Vav-cre Asxl1fl/fl*, *Vav-cre Tet2fl/fl*, and *Vav-cre Asxl1fl/flTet2fl/fl* cells are positive for CD45.2, whereas WT competitor cells are positive for CD45.1. On the right, monthly assessment of donor chimerism in the peripheral blood of recipient animals is shown up to 16 wk after transplant (*n* = 5 recipient mice were used for each genotype and experiment was performed in biological duplicate). 16-wk chimerism was significantly higher in *Tet2*^{−/−} transplanted mice compared with all other genotypes. (C) Representative FACS analysis of peripheral blood of mice transplanted with each genotype at 16 wk. Staining schemes are as indicated and parental gate was live cells. (D) Proportion of CD45.2+ peripheral blood cells of each lineage at 16 wk in mice transplanted with each genotype (*n* = 5 mice analyzed for each genotype) as determined by FACS analysis. Each competitive transplantation experiment was performed in biological duplicate with five recipient mice per genotype in each experiment. Error bars represent ±SD; *, P < 0.05 (Mann–Whitney *U* test).

2011; Quivoron et al., 2011). We analyzed the in vitro and in vivo phenotype of *Vav-cre Asxl1fl/fl Tet2fl/fl* hematopoietic cells compared with control, *Vav-cre Asxl1fl/fl*, and *Vav-cre Tet2fl/fl* mice (Fig. 6 A). Colony assays of whole BM cells from the same mice revealed reduced serial replating activity of *Asxl1* KO cells but restored serial-replating capacity of cells with compound *Asxl1/Tet2* loss (Fig. 6 A). More importantly, competitive transplantation experiments revealed a competitive advantage for *Vav-cre Asxl1fl/fl Tet2fl/fl* whole BM compared with matched CD45.1 competitor BM (Figs. 6, B–D). These data demonstrate that concurrent Tet2 loss restores the self-renewal defect induced by *Asxl1* loss.
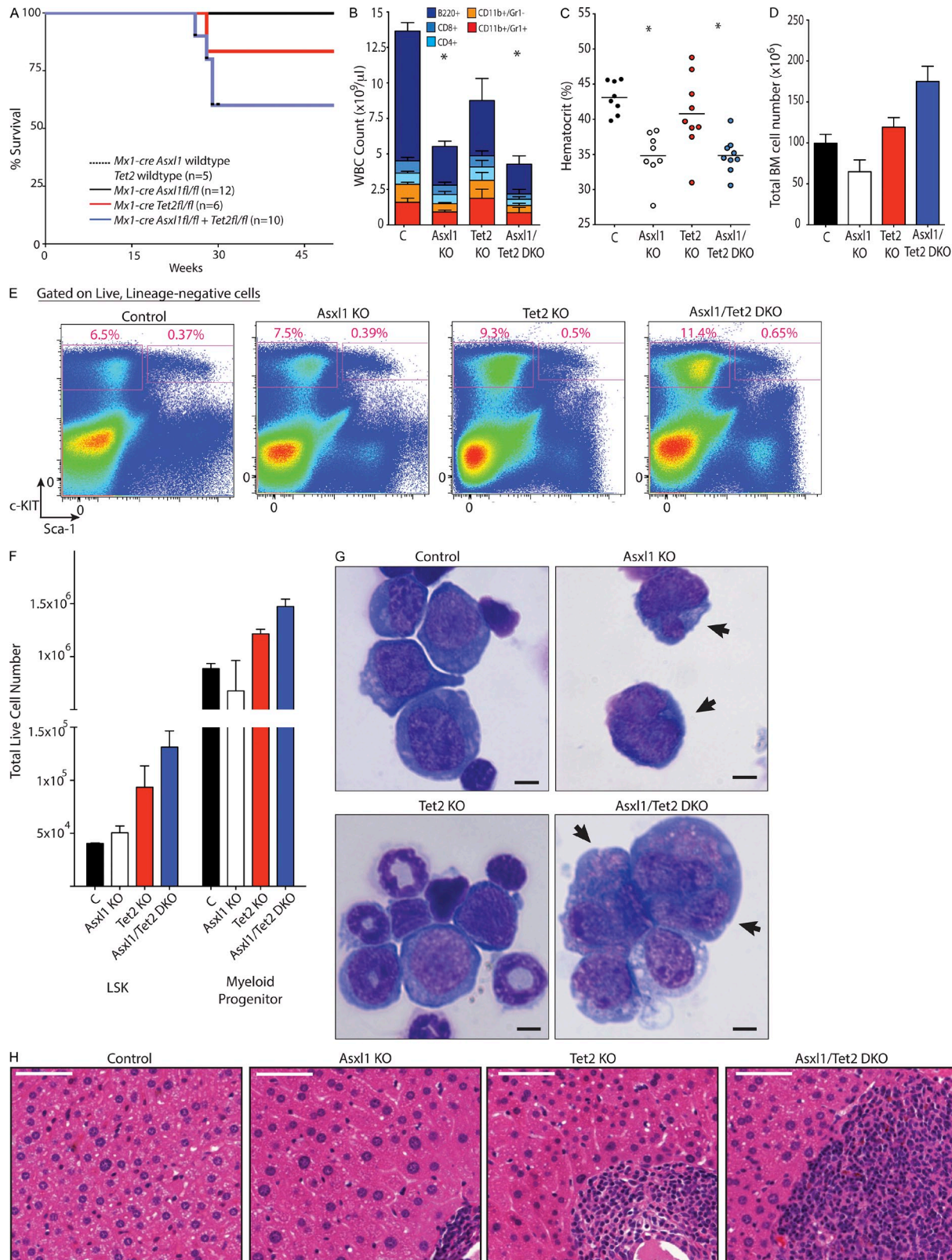
Figure 7. Concomitant deletion of *Asxl1* and *Tet2* results in myelodysplasia in mice. (A) Kaplan-Meier survival curve of primary Cre⁻ *Asxl1^{fl/fl}* (*n* = 5), *Mx1-cre Asxl1^{fl/fl}* (*n* = 12), *Mx1-cre Tet2^{fl/fl}* (*n* = 6), *Mx1-cre Asxl1^{fl/fl} Tet2^{fl/fl}* (*n* = 10 mice per genotype). Mice were treated with polyI:polyC at 4 wk after birth and then followed for 50 wk. (B) Peripheral WBC count and differential of recipient mice transplanted with BM from 6-wk-old *Mx1-cre Asxl1* WT *Tet2* WT (control; C), *Mx1-cre Asxl1^{fl/fl}* (Asxl1 KO), *Mx1-cre Tet2^{fl/fl}* (Tet2 KO), and *Mx1-cre Asxl1^{fl/fl} Tet2^{fl/fl}* (*Asxl1/Tet2* DKO) mice 66 wk after transplantation

Concomitant deletion of *Asxl1* and *Tet2* in vivo results in MDS
Given the restoration of self-renewal noted in mice with concomitant deletion of *Tet2* and *Asxl1* in the context of a competitive transplantation experiment, we investigated the phenotype of mice with compound deletion of *Tet2* and *Asxl1* compared with mice with deletion of each gene alone. A cohort of primary Cre⁻ *Asxl1*WT *Tet2*WT, *Mx1-cre Asxl1*^fl/fl (*Asxl1* KO), *Mx1-cre Tet2*^fl/fl (*Tet2* KO), and *Mx1-cre Asxl1*^fl/fl *Tet2*^fl/fl (double KO [DKO]) mice were treated with polyinosinic-polycytidylic acid (polyI:polyC) at 4 wk of life and followed up to 50 wk after birth (46 wk after polyI:polyC administration). At the end of this observation period, 40% of DKO mice (4/10) and 17.7% of Tet2 KO died (1/6), whereas no *Asxl1* KO (0/12) or control mice (0/5) died (Fig. 7 A).

For further analyses, to obtain a sufficiently large number of mice for each genotype, BM from 6-wk-old CD45.2 *Mx1-cre Asxl1* WT *Tet2* WT, *Mx1-cre Asxl1*^fl/fl (*Asxl1* KO), *Mx1-cre Tet2*^fl/fl (*Tet2* KO), and *Mx1-cre Asxl1*^fl/fl *Tet2*^fl/fl (DKO) mice were transplanted into lethally irradiated CD45.1 recipient mice (10 recipient mice per genotype). All recipient mice (including those transplanted with *Mx1-cre Asxl1* WT *Tet2* WT BM) were then treated with polyI:polyC 2 wk after transplantation to delete *Tet2* and/or *Asxl1*. At 72 wk after transplant, *Asxl1*-null and/or *Asxl1/Tet2* compound–null mice had significantly lower WBC counts and hematocrit compared with WT or *Tet2* single KO control mice (Fig. 7, B and C). As seen in mice with primary deletion of *Asxl1*, *Asxl1* KO mice here had reduced BM cellularity compared with control or *Tet2* KO mice (Fig. 7 D). However, despite the similar blood counts between *Asxl1* KO and DKO mice, the DKO had greater BM cellularity than mice with deletion of just *Asxl1* or even *Tet2* (Fig. 7 D). Examination of the HSPC compartment across mice with the four genotypes at 72 wk indicated a greater total number as well as relative frequency of LSK and MP cells in the BM of DKO mice compared with other groups (Fig. 7, E and F). Morphologically, BM of *Asxl1* KO mice was characterized by the presence of dysplastic erythroid precursor cells as seen in primary Asxl1 KO mice earlier (Fig. 7 G). The BM of DKO mice likewise was characterized by a similar presence of dysplastic erythroid precursors as well as dysplastic myeloid cells (Fig. 7 G) but lacked the hypocellularity seen in the BM of mice with Asxl1 deletion alone (Fig. 7 D). Histological analysis of liver tissue revealed increased hematopoietic cell infiltration in DKO mice compared with the other groups (Fig. 7 H). The presence

of morphological dysplasia in precursor cells, decrease in peripheral circulating mature cells, and concurrent increased total BM cells and HSPCs were suggestive of the presence of MDS in the *Asxl1/Tet2* compound–deficient mice.

Transcriptional effects of Asxl1 loss
To understand the basis for the impaired myeloid differentiation and self-renewal observed with *Asxl1* loss, we performed expression analysis of sorted LSK and MP cells from cytopenic 1-yr-old *Asxl1* KO mice and age-matched littermate controls (Fig. 8, A and B; and Tables S1 and S2). Analysis of RNA-Seq data identified a set of differentially expressed genes in Asxl1 KO LSK cells (797 genes) and MP cells (1,095 genes). Integrative analysis identified a set of 75 genes that were differentially expressed in Asxl1 KO LSK and MP cells, including 41 up-regulated and 34 down-regulated genes in Asxl1 KO mice relative to controls (Fig. 8 B).

Consistent with previous in vitro data (Abdel-Wahab et al., 2012), we observed increased expression of posterior *HoxA* genes in Asxl1 KO LSK cells, including *HoxA7* and *HoxA9* as well as the *Hox*-associated transcription factors *Hes5* and *Gdf11* (Fig. 8 C). *Meis1* was not up-regulated, with Asxl1 loss consistent with a previous study in in vitro systems (Fig. 8 C; Abdel-Wahab et al., 2012). We also noted a progressive, age-dependent increase $p16^{INK4a}$ expression in LT-HSCs and multipotent progenitor (MPP) cells (LSK CD48⁺ CD150⁻) of Asxl1 KO mice compared with age-matched controls (Fig. 8 D). The $p16^{INK4a}$ locus is a known PRC2 target (Jacobs et al., 1999; Bracken et al., 2007; Hidalgo et al., 2012; Tanaka et al., 2012), and in vitro loss of Asxl1 has been linked to defective Polycomb repression and reduced H3K27 methylation (Abdel-Wahab et al., 2012). Given the increase in $p16^{INK4a}$ expression in KO MPP cells from *Asxl1* KO mice, we examined the in vivo cell proliferation of MPP cells from 72-wk-old *Asxl1* KO (*Vav-cre Asxl1*^fl/fl) versus control mice (Cre⁻ *Asxl1*^fl/fl) via an in vivo BrdU incorporation assay. The MPP cells of *Asxl1* KO mice showed a significant decrease in S-phase compared with littermate control cells (Fig. 8 E). Flow cytometric quantitative assessment of apoptosis in LSK cells of the same mice revealed a significant increase in Annexin-V⁺/DAPI⁻ and Annexin-V⁺/DAPI⁺ LSK cells (Fig. 8 F; *n* = 5 mice per group) consistent with cell cycle exit and an increase in apoptosis in vivo.

To understand what transcriptional differences might exist between mice with compound deletion of Asxl1 and Tet2

(68 wk after polyI:polyC administration to recipient mice; *n* = 10 mice per genotype). Differential was determined by flow cytometric analysis of peripheral blood. (C and D) Hematocrit (C) and total number (D) of nucleated BM cells of same mice as shown in B. Horizontal lines indicate the mean. (E) Representative flow cytometric assessment of relative frequencies of MP and LSK cells in 72-wk-old mice. Parent population was live, lineage⁻ cells. (F) Total numbers of LSK and MP cells (lineage⁻ Sca-1⁻ c-Kit⁺) in mice from each genotype at 72 wk of age. This was determined by flow cytometric quantification of living LSK and MP cells from c-KIT–enriched BM cells harvested from spine plus bilateral femurs, tibiae, and humeri of each mouse from each genotype at 72 wk of age (*n* = 3 mice per group). (G) Wright-Giemsa stain of BM representative erythroid precursor from cytospins of 72-wk-old control, Asxl1 KO, Tet2 KO, or Asx1/Tet2 DKO mice. Arrows indicate multinuclearity and nuclear fragmentation in erythroid precursors. (H) Representation histological sections of liver from 72-wk-old control, Asxl1 KO, Tet2 KO, or Asx1/Tet2 DKO mice Bars: (G) 5 µm; (H) 50 µm. For A and B, *n* = 10 mice per group; for C–H, *n* = 3 mice per group. Error bars represent ±SD; *, P < 0.05 (Mann–Whitney *U* test).

JEM
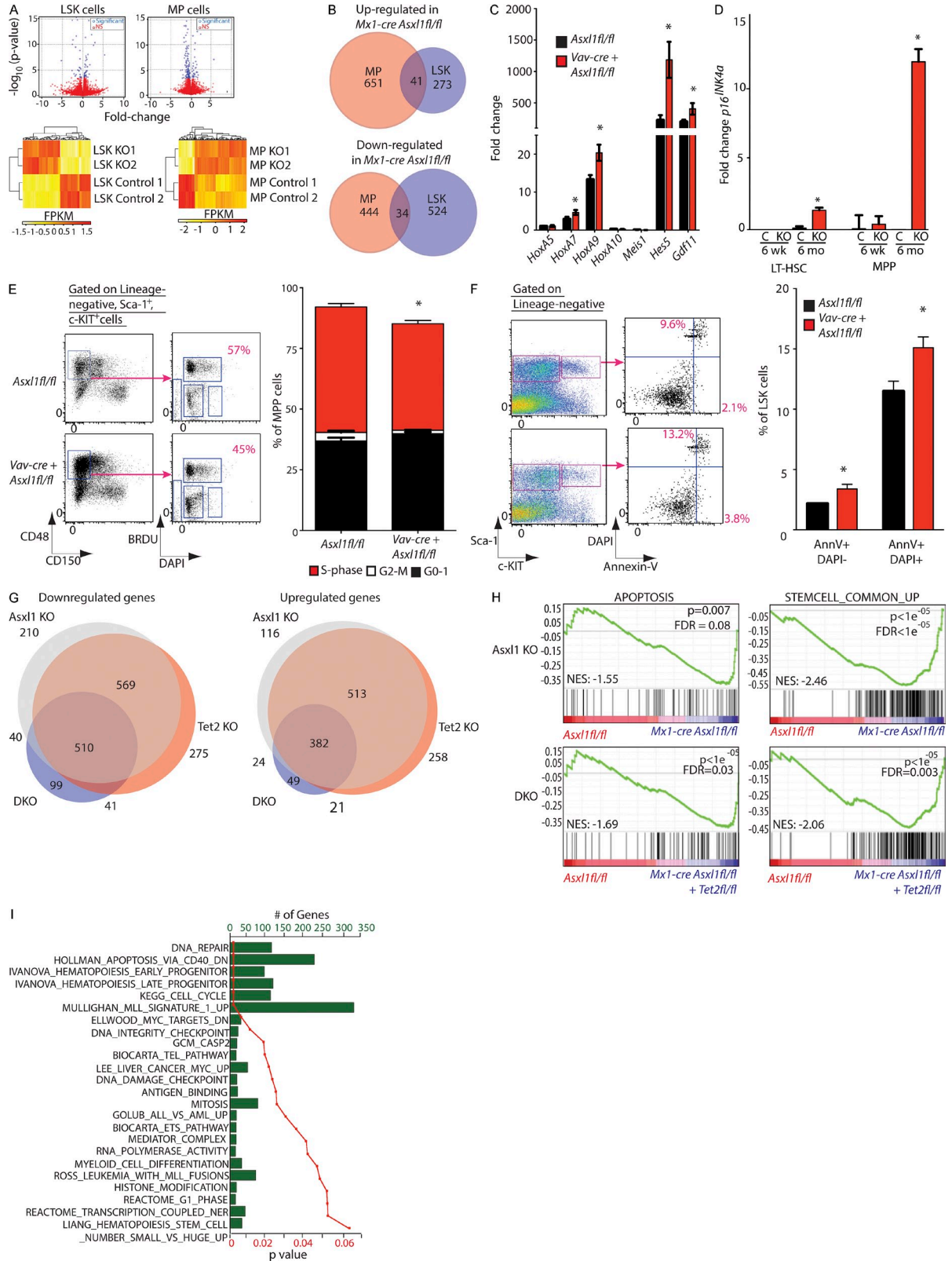
Figure 8. Identification of genes significantly dysregulated with deletion of *Asxl1* alone and in concert with deletion of *Tet2* and their functional impact. (A) Volcano plot of differentially expressed transcripts from RNA-Seq data of 1-yr-old control versus littermate *Asxl1* KO (*Mx1-cre Asxl1fl/fl*) LSK and MP (lineage⁻ Sca-1⁻ c-Kit⁺) cells (experiment included cells from two individual mice per genotype). (B) Venn diagrams of genes significantly up- and down-regulated with Asxl1 loss in LSK and MP (lineage⁻, Sca-1⁻, cKit⁺) cells from 1-yr-old *Mx1-cre Asxl1^{fl/fl}* mice and littermate

relative to mice with deletion of *Asxl1*, *Tet2*, or neither gene, we performed RNA-Seq on LSK cells sorted from the BM of 6-wk-old *Mx1-cre Asxl1* WT *Tet2* WT, *Mx1-cre Asxl1^fl/fl^*, *Mx1-cre Tet2^fl/fl^*, and *Mx1-cre Asxl1^fl/fl^ Tet2^fl/fl^* mice (Fig. 8 G and Table S3). Of the 1,744 genes significantly up-regulated in any KO mice relative to controls, the majority of these genes were shared between Asxl1 KO and Tet2 KO LSKs but not DKO LSKs (32.6% of up-regulated genes [569/1,744 genes]), followed by genes shared between Asxl1 KO, Tet2 KO, and DKO mice (29.2% of up-regulated genes [510/1,744 genes]). Likewise, for the 1,363 significantly down-regulated genes, the majority of these were shared between Asxl1 KO and Tet2 KO LSKs but not DKO LSKs (37.6% of up-regulated genes [513/1,363 genes]), followed by genes shared between Asxl1 KO, Tet2 KO, and DKO mice (28.0% of up-regulated genes [382/1,363 genes]).

We next performed gene set enrichment analysis (GSEA) to identify gene sets enriched in HSPCs from Asxl1 KO mice or Asxl1/Tet2 DKO mice compared with other groups (Subramanian et al., 2005). We identified gene sets enriched in HSCs (Ramalho-Santos et al., 2002) and apoptosis (http://www.genome.jp/kegg/pathway/hsa/hsa04210.html) in mice with *Asxl1* deletion and with concomitant *Asxl1/Tet2* deletion (Fig. 8 H). We also identified gene sets that were uniquely enriched in *Tet2/Asxl1* DKO mice and not seen in the other groups. This prominently included gene sets characteristic of apoptosis signatures, purified HSPCs (Ivanova et al., 2002), cell cycle regulators (http://www.genome.jp/kegg/pathway/hsa/hsa04110.html), and signatures from *MLL*-rearranged primary leukemias (Fig. 8 I; Ross et al., 2003; Mulligan et al., 2007).

Genome–wide binding of Asxl1 and global effects of Asxl1 loss on the epigenome

Asxl1 has been shown to interact with epigenetic modifiers known to impact transcription (Abdel-Wahab et al., 2012; Dey et al., 2012). This includes binding to the core members of the PRC2, where loss of *ASXL1* has previously been found to result in global down-regulation of histone H3 lysine 27 (H3K27) methylation (Abdel-Wahab et al., 2012) in vitro and in ex vivo *ASXL1* mutant primary patient samples. Consistent with this, H3K27 trimethyl (H3K27me3) levels were significantly reduced after *Asxl1* deletion (Fig. 9 A) despite sustained expression of the core PRC2 components (Fig. 9 B).

Although the effects of Asxl1 loss on transcription caused by alterations in histone posttranslational modifications have previously been described (Abdel-Wahab et al., 2012), direct transcriptional targets of Asxl1 through characterization of Asxl1 binding throughout the genome have never previously been assessed. We therefore performed chromatin immunoprecipitation (ChIP) for Asxl1 followed by DNA sequencing (ChIP-Seq) in purified mouse myeloid hematopoietic cells. Asxl1 was found to bind to many sites throughout the genome with the majority of significantly enriched Asxl1 peaks (78%) located at CpG-rich transcription start sites (TSSs; Fig. 9, C–E; and Tables S4 and S5). Motif enrichment analysis of the Asxl1–binding sites revealed that the top occurring motifs are most similar to known binding sites of the Ets family of transcription factors (Fig. 9 F; P = 1 × 10⁻⁵⁹, percent target = 40.1%, and percent background = 21.4%). A significant subset of genes with dysregulated expression in Asxl1 KO LSK/MP cells were confirmed as direct targets of Asxl1 in our ChIP-Seq analysis (14 up-regulated and 9 down-regulated genes; Table 1).

DISCUSSION

Here we show that conditional deletion of *Asxl1*, a gene commonly mutated in human MDS, in hematopoietic cells resulted in the development of progressive anemia and leukopenia with concomitant multilineage myeloid dysplasia in vivo. *Asxl1* deletion was associated with an increase in the frequency and total number of HSPCs, increased apoptosis, and altered cell cycle distribution of HSPCs in vivo. Asxl1 loss also led to a reduction in myeloid colony output. MDS is characterized by variable cytopenias caused by ineffective production of mature granulocyte, erythroid, and/or megakaryocyte populations and a risk of transformation to AML. Functional characterization of primary samples from patients with MDS has identified an expansion of the primitive HSC compartment (comprised of long-term and short-term HSCs; Will et al., 2012; Pang et al., 2013), the presence of specific genetic alterations throughout the diseased clone originating in the most immature HSCs (Nilsson et al., 2000, 2007; Tehranchi

---

Cre⁻ controls as identified in A. (C) qRT-PCR analysis of *HoxA* and *Hox*-associated transcription factor genes in LSK cells of 1-yr-old Cre⁻ *Asxl1^fl/fl^* control versus littermate *Vav-cre Asxl1^fl/fl^*. (D) qRT-PCR analysis of *p16^INK4a^* in LT-HSCs (lineage⁻, Sca-1⁺, c-Kit⁺, CD150⁺, CD48⁻) and MPP cells (lineage⁻, Sca-1⁺, c-Kit⁺, CD150⁻, CD48⁺) from 6-wk- and 6-mo-old control (C) versus littermate *Vav-cre Asxl1^fl/fl^* (KO) mice. (E) Cell cycle analysis of MPPs from 72-wk-old *Vav-cre Asxl1^fl/fl^* or littermate Cre⁻ *Asxl1^fl/fl^* control mice with in vivo BrdU administration. Representative FACS plot analysis showing gating on MPP cells followed by BrdU versus DAPI stain is shown on the left (parent gate is LSK cells). Relative quantification of the percentage of MPP cells in S, G2/M, and G0/1 phase is shown on the right (n = 5 mice per group). (F) Assessment of the proportion of HSPCs undergoing apoptosis was performed by Annexin V/DAPI stain of LSK cells from 72-wk-old *Vav-cre Asxl1^fl/fl^* mice or Cre⁻ *Asxl1^fl/fl^* littermate controls. Representative FACS plot analysis showing gating on LSK cells followed by Annexin V versus DAPI stain is shown on the left (parent gate is lineage⁻ cells). Relative quantification of the percentage of Annexin V⁺/DAPI⁻ and Annexin V⁺/DAPI⁺ LSK cells is shown on the right (n = 5 mice per group). (G) Comparison of significant differentially expressed genes in LSK cells from 6-wk-old *Mx1-cre Asxl1^fl/fl^*, *Mx1-cre Tet2^fl/fl^*, or *Mx1-cre Asxl1^fl/fl^ Tet2^fl/fl^* relative to controls (or *Mx1-cre Asxl1* WT *Tet2* WT). 99 genes are uniquely down-regulated in *Asxl1/Tet2* DKO mice relative to all other genotypes (left), whereas 49 genes are significantly up-regulated (right). (H) GSEA of overlapping and statistically significant gene sets enriched in the LSK cells of mice with deletion of *Asxl1* alone or with combined *Asxl1* and *Tet2* deletion. (I) Gene sets uniquely enriched in mice with concomitant deletion of *Asxl1* and *Tet2* relative to all other genotypes as determined by GSEA. Error bars represent ±SD; *, P < 0.05 (Mann–Whitney *U* test).
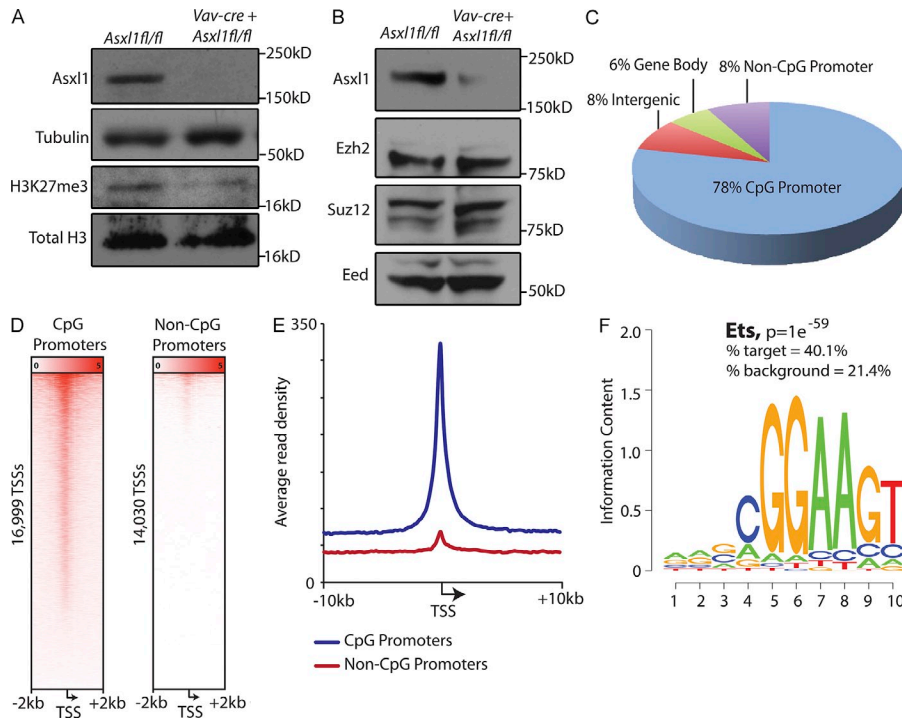
Figure 9. Effect of *Asxl1* loss in vivo on H3K27me3 and identification of Asxl1–regulated genes ChIP-Seq. (A) Western blot analysis of H3K27me3 and total histone H3 in splenocytes of 6-wk-old *Vav-cre Asxl1^{fl/fl}* mice relative to littermate control. (B) Levels of core PRC2 members Ezh2, Suz12, and Eed in splenocytes of same mice as shown in A. (C) Characterization of Asxl1-binding sites identified by anti-Asxl1 ChIP-Seq analysis in mouse WT BMDMs. (D) Heat map representation of Asxl1 ChIP-Seq signal centered around TSSs (±2 kb) of CpG (left) and non-CpG (right) promoters. (E) Mean Asxl1 ChIP-Seq signal density of CpG and non-CpG promoters centered around the TSS ± 10 kb. (F) Motif enrichment analysis of Asxl1-binding sites identified significant enrichment of Ets transcription factor binding sites (P = 1×10^{-59}, percent target = 40.1%, and percent background = 21.4%).

et al., 2010; Will et al., 2012; Pang et al., 2013), dysplastic clonogenic activity of HSCs with reduced in vitro colony formation from MDS-derived HSCs (Sawada et al., 1993, 1995; Will et al., 2012), and an increase in the frequency and absolute number of HSPCs in the setting of decreased mature circulating cells with a concomitant increase in apoptosis of HSPCs in MDS patients (Sawada et al., 1993, 1995; Pang et al., 2013). Collectively, the phenotype of *Asxl1* loss recapitulates these central features of human MDS.

One aspect of the *Asxl1* conditional KO mouse model that differs from human MDS is the BM hypocellularity observed in *Asxl1* KO mice, in contrast to the increased BM cellularity in most MDS patients. Nevertheless, the impaired production of mature myeloid and erythroid cells in the context of an increased relative and total numbers of HSPCs in *Asxl1* conditional KO mice does recapitulate key features of human MDS. Moreover, concomitant loss of *Asxl1* and *Tet2*, which are commonly mutated in concert in human MDS, resulted in increased BM cellularity and disease severity with pathological evidence of multilineage dysplasia.

In contrast to MPN and AML, there are few previously described models of MDS, and to date no models of MDS based on mutations in recurrently mutated MDS disease alleles. The most widely used model of MDS is based on transgenic expression of a *NUP98-HOXD13* fusion allele (Lin et al., 2005). Although this model has many of the characteristic features of human MDS, the *NUP98-HOXD13* fusion was identified in a young patient with therapy–related AML (Raza-Egilmez et al., 1998) and has not been identified in MDS patients to date. In contrast, *ASXL1* mutations occur in 15–20% of patients with MDS.

Prior studies of the effects of *Asxl1* loss on development and hematopoiesis were performed using a constitutive *Asxl1* KO mouse model (Fisher et al., 2010a,b). Our conditional model allows for evaluation of the effects of postnatal deletion of *Asxl1* and obviates the problems associated with a high frequency of perinatal lethality in mice with constitutive *Asxl1* deletion. Notably, Fisher et al. (2010a,b) identified a 72% reduction in the expected number of *Asxl1* homozygous KO mice by postnatal day 21; when mice were backcrossed more than eight generations to a consistent genetic background, KO mice were 100% embryonic lethal, preventing analysis of adult constitutive *Asxl1* KO mice. Similar to the germline model, we observed an age-dependent decrease in mature B lymphocytes, splenomegaly caused by EMH, and decreased formation of myeloid and erythroid colonies from *Asxl1* KO cells (Fisher et al., 2010a,b). In addition, Fisher et al. (2010a,b) observed dysregulated expression of *HoxA* genes and homeotic transformation of homozygous *Asxl1* mutant embryos, consistent with the current *Asxl1* germline and conditional KO models described in this study.

Despite these similarities, several differences exist between the two models. First, no reproducible differences in peripheral blood counts, BM cellularity, or BM cell morphology were seen in *Asxl1* constitutive KO mice. In contrast, mice with conditional, homozygous, postnatal deletion of *Asxl1* developed leukopenia, anemia, myeloerythroid dysplasia, and BM hypocellularity starting at 6 mo of life. This could be caused by differences in the strain of the mice analyzed, the timing of *Asxl1* loss, or cell–nonautonomous effects observed in the constitutive KO model.

Of note, the more profound hematologic abnormalities seen with serial competitive and noncompetitive transplantation

Table 1. Genes directly regulated by Asxl1 as determined by differential expression in HSPCs with *Asxl1* deletion and directly bound by Asxl1

Gene	MPs		LSK cells		Anti–Asxl1 ChIP-Seq		
	log₂ (fold change)	P–value	log₂ (fold change)	P–value	Peak p-value	Fold enrichment	Peak FDR
Tmem87a	3.91	9.60×10^{-6}	3.11	3.68×10^{-6}	2.78×10^{-7}	4.21	0.29
Pusl1	1.54	2.21×10^{-7}	1.30	1.29×10^{-3}	3.04×10^{-8}	5.24	0.15
Ddx23	1.45	1.15×10^{-10}	1.09	1.79×10^{-3}	7.45×10^{-15}	6.93	0.09
Pan3	1.01	1.36×10^{-5}	0.79	8.21×10^{-4}	4.49×10^{-29}	9.3	0
Srrm2	0.86	6.02×10^{-8}	0.98	1.61×10^{-6}	1.85×10^{-12}	4.49	0.06
Dusp6	0.80	4.11×10^{-4}	0.63	2.45×10^{-3}	4.48×10^{-30}	8.43	0
Cdca2	0.77	6.77×10^{-8}	0.62	3.84×10^{-4}	3.78×10^{-8}	3.6	0.16
Apobec3	0.54	2.25×10^{-10}	0.36	8.29×10^{-4}	4.48×10^{-10}	6.18	0.09
Cdc40	0.41	1.68×10^{-4}	0.59	1.93×10^{-5}	4.79×10^{-10}	5.91	0.09
Rpl30	0.39	1.73×10^{-10}	0.31	5.74×10^{-5}	1.57×10^{-22}	6.99	0
Rad51	0.39	3.17×10^{-3}	0.51	3.48×10^{-3}	2.28×10^{-10}	7.16	0.1
Nbr1	0.34	4.65×10^{-8}	0.43	0.00	4.04×10^{-19}	5.69	0
Slc24a6	0.30	4.66×10^{-4}	0.82	3.24×10^{-10}	7.52×10^{-11}	8.09	0.1
Dhrs3	0.28	4.27×10^{-3}	0.37	2.16×10^{-4}	4.33×10^{-49}	5.15	0
Cdk2	0.23	1.51×10^{-4}	0.21	3.94×10^{-4}	1.06×10^{-16}	7.89	0.11
Ifngr1	0.18	4.59×10^{-3}	0.38	1.99×10^{-4}	3.02×10^{-20}	11.89	0
Hsp90ab1	0.16	1.08×10^{-3}	0.24	9.11×10^{-5}	1.41×10^{-45}	12.71	0
Mtmr9	−0.44	4.53×10^{-4}	−0.47	3.62×10^{-4}	4.07×10^{-11}	7.19	0.11
Ppp1cb	−0.48	1.35×10^{-8}	−0.64	2.14×10^{-7}	5.79×10^{-12}	4.77	0.09
Mthfr	−0.51	1.65×10^{-3}	−0.47	1.21×10^{-3}	2.47×10^{-9}	4.82	0.11
Ncf4	−0.52	7.21×10^{-9}	−0.66	4.38×10^{-5}	2.16×10^{-18}	7.53	0.07
Slc25a19	−0.96	7.68×10^{-11}	−0.75	3.50×10^{-6}	2.24×10^{-7}	6.64	0.28
Rpl29	−1.18	0.00	−0.76	0.00	2.47×10^{-9}	5.96	0.11
Mettl23	−1.33	8.43×10^{-10}	−1.10	1.21×10^{-5}	1.10×10^{-7}	3.68	0.2
Caskin2	−1.54	3.42×10^{-5}	−2.45	1.53×10^{-4}	4.97×10^{-13}	5.6	0.07
Thbs1	−1.75	4.71×10^{-7}	−1.84	1.63×10^{-6}	9.53×10^{-8}	5.06	0.19

FDR, false discovery rate. Differentially expressed genes in RNA sequencing of MPs (lineage⁻ Sca-1⁻ c-KIT⁺ cells) from 1-yr-old *Mx1-cre Asxl1^{fl/fl}* mice relative to Cre⁻ *Asxl1^{fl/fl}* littermate controls. Differentially expressed genes in RNA sequencing of LSK cells (lineage⁻ Sca-1⁺ c-KIT⁺ cells) from 1-yr-old *Mx1-cre Asxl1^{fl/fl}* mice relative to Cre⁻ *Asxl1^{fl/fl}* littermate controls. Data derived from anti-Asxl1 ChIP-Seq in WT C57BL/6H BMDMs.

of *Asxl1* conditional KO hematopoietic cells here have no counterpart in the study of the prior constitutive KO model as serial transplantation was not performed in the prior study (Fisher et al., 2010b). The marked impairment in serial transplantability observed with *Asxl1* loss is consistent with the progressive defects in HSC function observed in mice with other alterations in other Polycomb group functions (Ohta et al., 2002).

Although noncompetitive transplantation experiments demonstrated that the MDS phenotype was cell autonomous, Asxl1 deficiency was associated with a defect in HSC self-renewal in competitive transplantation assays and in in vitro colony formation. These data suggested that concurrent genetic or epigenetic alterations in *ASXL1* mutant MDS cells must promote self-renewal to allow for clonal dominance of MDS cells. Indeed, concurrent *Tet2* loss restored the self-renewal defect induced by *Asxl1* loss. Moreover, mice with concomitant loss of *Asxl1* and *Tet2* developed a larger increase in HSPCs,

increased BM cellularity, and decreased numbers of circulating mature cells compared with single-gene KO mice. This phenotype is consistent with more severe MDS and suggests a functional interdependency between these two disease alleles in MDS. Subsequent studies may identify additional disease alleles that can rescue the self-renewal defect seen in *ASXL1*-deficient stem cells and may lead to the identification of additional mutational interdependencies in MDS and in other malignant contexts.

We previously demonstrated that loss of *ASXL1* in vitro results in global down–regulation in H3K27me3 (Abdel-Wahab et al., 2012), the repressive histone modification placed by the PRC2. Here we demonstrate that *Asxl1* deletion in the hematopoietic compartment results in reduced H3K27me3 in vivo. We used ChIP-Seq for Asxl1 itself to show that Asxl1 is enriched at gene promoter regions throughout the genome, suggesting a potential role for Asxl1 in direct regulation of gene transcription. In addition, motif enrichment analysis of

Asxl1-binding sites revealed enrichment in known binding sites of the Ets family of transcription factors. The significant overlap between genome-wide binding of *Asxl1* and Ets family members is critically supportive of the importance of Asxl1 in hematopoiesis as the Ets family of transcription factors are very well understood to play a key role in the growth, survival, differentiation, and activation of hematopoietic cells (Mizuki et al., 2003; Vangala et al., 2003; Koschmieder et al., 2005; Steidl et al., 2006; Choi et al., 2008). Deletion, mutation, and translocation of ETS family members are well-described in myeloid malignancies (Gilliland, 2001), including *ETV6* mutations/translocations in MDS and chronic myelomonocytic leukemia (Haferlach et al., 2012) and loss-of-function mutations of *PU.1* in AML (Mueller et al., 2002). Moreover, common oncogenic events seen in patients with myeloid malignancies have been demonstrated to transform myeloid cells through suppression of expression of key Ets members. For example, *FLT3-ITD* mutations and the AML1–ETO (t(8;21)) fusion oncoprotein have been shown to suppress PU.1 expression and function (Mizuki et al., 2003; Vangala et al., 2003). In addition, down-regulation of PU.1 expression results in impaired myeloid differentiation (Rosenbauer et al., 2004; Steidl et al., 2006). Further work to understand the involvement of individual Ets family members and/or a shared transcriptional program between Asxl1 loss and Ets family member loss (Steidl et al., 2006) in the pathogenesis of *ASXL1* mutant myeloid malignancy will be critical.

Collectively, our experiments reveal that deletion of *Asxl1* results in craniofacial and skeletal developmental abnormalities and mice with hematopoietic-specific *Asxl1* loss developed hallmark features of MDS, including progressive ineffective hematopoiesis, impaired myeloid differentiation, multilineage dysplasia, and increased apoptosis and altered cell cycle regulation of HSPCs. Given the paucity of mouse models of human MDS based on known, recurrent MDS disease alleles, we believe the development of a genetically accurate model of MDS will inform subsequent studies aimed to elucidate the molecular basis for MDS and to develop novel therapies for MDS patients.

MATERIALS AND METHODS

Animals. All animals were housed at New York University School of Medicine or at Memorial Sloan-Kettering Cancer Center. All animal procedures were conducted in accordance with the Guidelines for the Care and Use of Laboratory Animals and were approved by the Institutional Animal Care and Use Committees at New York University School of Medicine and Memorial Sloan-Kettering Cancer Center.

Generation of *Asxl1*-deficient mice. The *Asxl1* allele was deleted by targeting exons 5–10. Two *LoxP* sites flanking exon 5–10 and an *Frt*-flanked neomycin selection cassette were inserted in the upstream intron (Fig. 1 A). 10 µg of the targeting vector was linearized by NotI and then transfected by electroporation of BAC-BA1 (C57BL/6 × 129/SvEv) hybrid ES cells. After selection with G418 antibiotic, surviving clones were expanded for PCR analysis to identify recombinant ES clones. Secondary confirmation of positive clones identified by PCR was performed by Southern blotting analysis. DNA was digested with BamHI and electrophoretically separated on a 0.8% agarose gel. After transfer to a nylon membrane, the digested DNA was hybridized with a probe targeted against the 3′ or 5′ external region. DNA from C57BL/6 (B6), 129/SvEv (129), and BA1 (C57BL/6 × 129/SvEv;

Hybrid) mouse strains was used as WT controls. Positive ES clones were expanded and injected into blastocysts.

The generated mice (*Asxl1*$^{fl/fl}$) were initially crossed to a germline *Flp*-deleter (The Jackson Laboratory), to eliminate the neomycin cassette, and subsequently to the IFN-α–inducible *Mx1-cre* (The Jackson Laboratory), the hematopoietic-specific *Vav-cre*, and the germline *EIIa-cre* (Kühn et al., 1995; Lakso et al., 1996; Stadtfeld and Graf, 2005). Mice were backcrossed for six generations to C57BL/6 mice.

Asxl1$^{fl/fl}$, *Asxl1*$^{fl/+}$, and *Asxl1*$^{+/+}$ littermate mice were genotyped by PCR with primers Asxl1-F3 (5′-CAGCCGTTTTACCACAGTTT-3′) and Asxl1-R3 (5′-AGGGAAAGGGACAGAATGAC-3′) using the following parameters: 95°C for 4 min, followed by 35 cycles of 95°C for 45 s, 56°C for 45 s, and 72°C for 1 min, and then 72°C for 5 min. The WT allele was detected as a band at 200 bp, whereas the floxed allele was detected as a band of 380 bp. Excision after Cre recombination was confirmed by PCR with primers to detect a floxed portion of the construct (Asxl1-RecF, 5′-ACG-CCGGCTTAAGTGTACACG-3′; and Asxl1-RecR, 5′-GACTAAGTT-GCCGTGGGTGCT-3′) using the same parameters as above.

In vivo experiments. *Mx1-cre Asxl1*$^{fl/fl}$ conditional and Cre$^-$ *Asxl1*$^{fl/fl}$ control mice received five intraperitoneal injections of polyI:polyC every other day at a dose of 20 mg/kg of body weight starting at 2 wk after birth. For the hematopoietic-specific *Vav-cre* line, Asxl1$^{fl/fl}$*Vav-cre*$^+$, and Asxl1$^{fl/fl}$*Vav-cre*$^-$ mice were analyzed between 3 and 60 wk of age. BM, spleen, and peripheral blood were analyzed by flow cytometry. Formalin-fixed paraffin-embedded tissue sections were stained with hematoxylin and eosin (H&E). Peripheral blood was smeared on a slide and stained using the Wright-Giemsa staining method. Tissue sections and blood smears were evaluated by a hematopathologist (C.Y. Park) Deletion of the *Asxl1* allele and transcript was measured by genomic PCR and Western blot analysis.

BM transplantation. Freshly dissected femurs and tibias were isolated from *Asxl1*$^{fl/fl}$ CD45.2$^+$ or *Vav-cre*$^+$*Asxl1*$^{fl/fl}$ CD45.2$^+$ mice. BM was flushed with a 3-cc insulin syringe into PBS supplemented with 3% fetal bovine serum. The BM was spun at 0.5 g by centrifugation at 4°C, and RBCs were lysed in ammonium chloride-potassium bicarbonate lysis buffer for 5 min. After centrifugation, cells were resuspended in PBS plus 3% FBS, passed through a cell strainer, and counted. Finally, 0.5×10^6 total BM cells of *Asxl1*$^{fl/fl}$ CD45.2$^+$ or *Vav-cre*$^+$ *Asxl1*$^{fl/fl}$ CD45.2$^+$ mice were mixed with 0.5×10^6 WT CD45.1$^+$ support BM and transplanted via tail vein injection into lethally irradiated (two times 450 cGy) CD45.1$^+$ host mice. Chimerism was measured by FACS in peripheral blood at 4 wk after transplant (week 0, pre-polyI:polyC). Chimerism was followed via FACS in the peripheral blood every 4 wk (week 0, 4, 6, 8, 12, and 16 after polyI:polyC injection). Additionally, for each bleeding, whole blood cell counts were measured on a blood analyzer, and peripheral blood smears were scored. Chimerism in the BM, spleen, and thymus was evaluated at 16 wk via animal sacrifice and subsequent FACS analysis. The above procedure was also repeated with *Asxl1*$^{fl/fl}$ CD45.2$^+$, *Vav-cre*$^+$ *Asxl1*$^{fl/fl}$ CD45.2$^+$, *Vav-cre*$^+$ *Tet2*$^{fl/fl}$ CD45.2$^+$, and *Vav-cre*$^+$ *Asxl1*$^{fl/fl}$ *Tet2*$^{fl/fl}$ CD45.2$^+$ mice for competitive transplantation of mice with loss of Asxl1, Tet2, or both. For noncompetitive transplantation experiments, 10^6 total BM cells of *Asxl1*$^{fl/fl}$ CD45.2$^+$, littermate *Vav-cre*$^+$ *Asxl1*$^{fl/fl}$ CD45.2$^+$, or littermate *Mx1-cre*$^+$ *Asxl1*$^{fl/fl}$ CD45.2$^+$ mice were injected into lethally irradiated (two times 450 cGy) CD45.1$^+$ host mice. Similarly, for LSK transplants, 1,000 FACS-sorted LSK cells from secondarily transplanted *Asxl1* KO or control mice were transplanted into lethally irradiated CD45.1 host mice. Recipient mice were then followed until moribund or 80 wk after transplantation.

In vitro colony-forming assays. LSK, CMP, GMP, and MEP cells were sorted from the BM of *Asxl1*$^{fl/fl}$ and littermate *Vav-cre*$^+$ *Asxl1*$^{fl/fl}$ mice and seeded at a density of 500 cells/replicate for LSK cells and 1,000 cells/replicate for CMP, GMP, and MEP subsets into cytokine-supplemented methylcellulose medium (Methocult M3434; STEMCELL Technologies). Colonies propagated in culture were scored at day 7. Representative colonies were isolated from the plate for cytospins. Remaining cells were resuspended and

counted, and a portion was taken for replating (20,000 cells/replicate) for a total of seven platings. Cytospins were performed by resuspending in warm PBS and spun onto the slides at 350 *g* for 5 min. Slides were air-dried and stained using the Giemsa–Wright method.

Antibodies, FACS, and Western blot analysis. Antibody staining and FACS analysis was performed as previously described (Klinakis et al., 2011). BM or spleen mononuclear cells were stained with a lineage cocktail comprised of antibodies targeting CD4, CD8, B220, NK1.1, Gr-1, CD11b, Ter119, and IL-7Rα. Cells were also stained with antibodies against c-Kit, Sca-1, FcγRII/III, and CD34. Cell populations were analyzed using a FACS-LSRII (BD) and sorted with a FACSAria instrument (BD). All antibodies were purchased from BD or eBioscience. We used the following antibodies: c-Kit (2B8), Sca-1 (D7), Mac-1/CD11b (M1/70), Gr-1 (RB6-8C5), NK1.1 (PK136), Ter-119, IL7-Rα (A7R34), CD34 (RAM34), FcγRII/III (2.4G2), CD4 (RM4-5), CD4 (H129.19), CD8 (53-6.7), CD45.1 (A20), CD45.2 (104), CD150 (9D1), and CD48 (HM48-1). The following antibodies were used for Western blot analysis: Asxl1 (clone N-13; Santa Cruz Biotechnology, Inc.), Ezh2 (EMD Millipore), Suz12 (Abcam), EED (Abcam), H3K27me3 (Abcam), total H3 (Abcam), and tubulin (Sigma-Aldrich).

Cell cycle and apoptosis analyses. For cell cycle analysis, the BrdU–APC kit was used (BD) according to the manufacturer's protocol. Mice were treated with 1 mg BrdU intraperitoneally, followed by harvest of BM cells 24 h later. For evaluation of apoptosis, the Annexin V–FITC apoptosis detection kit was used (BD) according to the manufacturer's recommendations. DAPI was used as counterstain in both BrdU and annexin V experiments.

Histological analyses. Mice were sacrificed and autopsied, and then dissected tissue samples were fixed for 24 h in 4% paraformaldehyde, dehydrated, and embedded in paraffin. Paraffin blocks were sectioned at 4 μm and stained with H&E. Images were acquired using an Axio Observer A1 microscope (Carl Zeiss).

Peripheral blood analysis. Blood was collected by retroorbital bleeding using heparinized microhematocrit capillary tubes (Thermo Fisher Scientific). Automated peripheral blood counts were obtained using a HemaVet 950 (Drew Scientific) according to standard manufacturer's instruction. Differential blood counts were realized on blood smears stained using Wright-Giemsa staining and visualized using an Axio Observer A1 microscope.

RNA-Seq and quantitative real-time PCR (qRT-PCR) analysis. Total RNA was isolated using the RNeasy Plus Mini kit (QIAGEN), and cDNA was synthesized using the SuperScript First-Strand kit (Invitrogen). Quantitative PCR was performed using SYBR green iMaster and a Light-Cycler 480 (Roche). For RNA-Seq analysis, Fastq files were aligned to mm9 using TopHatV1.4 with default parameters. Differential expression tests were performed using the Cuffdiff module of Cufflinks with RefSeq genes provided as an annotation (–N, -u and –M options engaged). We considered genes that had a q < 0.05 to be significantly different between genotypes.

ChIP-Seq and analysis. Because low chromatin yields from HSPC populations precluded ChIP-Seq experiments, BMDMs from WT C57BL/6 mice were used as a surrogate to identify genome-wide Asxl1 binding sites. The antibody used for Asxl1 ChIP-Seq experiments was obtained from Santa Cruz Biotechnology, Inc. ChIP was performed as described previously (Dey et al., 2012).

ChIP and input DNAs were prepared for amplification by converting overhangs into phosphorylated blunt ends and adding an adenine to the 3′ ends. Illumina adaptors were added and the library was size-selected (175–225 bp) on an agarose gel. The adaptor- ligated libraries were amplified for 18 cycles. The resulting DNA libraries were purified, quantified, and tested by qPCR at the same specific genomic regions as the original ChIP DNA to assess quality of the amplification reactions. DNA libraries then were sequenced on the Illumina Genome Analyzer II.

Sequenced reads were aligned to the reference genomes (mm9) using bowtie with maximum two mismatches, keeping only uniquely mapping reads. Peak calling was performed using MACS1.4 with the following options: -p 1e-7,–nomodel True,–shiftsize 100,–keep-dup 1. Peaks were assigned to genes using bedtools. We considered Asxl1-bound genes to be any mouse RefSeq entry containing a peak overlapping the gene or 2 kb upstream of the TSS. ChIP-Seq read profile and heat map densities were generated using genomic tools. Mouse RefSeq and CpG island annotations were downloaded from the UCSC Genome Bioinformatics Table Browser.

Skeletal preparations. Skeletal preparations were performed as described previously (de Pontual et al., 2011).

Online supplemental material. Table S1, included as a separate PDF file, shows differentially expressed transcripts between 1-yr-old *Mx1-cre* Asxl1$^{fl/fl}$ and Asxl1$^{fl/fl}$ LSK cells by RNA sequencing. Table S2, included as a separate PDF file, shows differentially expressed transcripts between 1-yr-old *Mx1-cre* Asxl1$^{fl/fl}$ and Asxl1$^{fl/fl}$ MPs by RNA sequencing. Table S3, included as a separate PDF file, shows differentially expressed genes in LSK cells from 6-wk-old *Mx1-cre Asxl1$^{fl/fl}$*, *Mx1-cre Tet2$^{fl/fl}$*, and *Mx1-cre Asxl1$^{fl/fl}$ Tet2$^{fl/fl}$*. Table S4, included as a separate PDF file, shows regions with significant Asxl1 binding by anti-Asxl1 ChIP-Seq. Table S5, included as a separate PDF file, shows genes with significant Asxl1 binding ±2 kb from the TSS as determined by anti-Asxl1 ChIP-Seq. Online supplemental material is available at http://www.jem.org/cgi/content/full/jem.20131141/DC1.

Author contributions: O. Abdel-Wahab, J. Gao, I. Aifantis, and R.L. Levine designed the study. O. Abdel-Wahab, J. Gao, M. Adli, Y.R. Chung, J.Y. Shin, P.K. Bhatt, O.A. Guryanova, E. Kim, L. Telis, and S. Pandey performed the experiments. D. Ndiaye-Lobry, LM. LaFave, A.H. Shih, and S. Pandey helped with animal generation, genotyping, and maintenance. S. Monette and C.Y. Park performed phenotypic and histological analysis of tissues. M. Adli, A. Dey, T. Trimarchi, R. Koche, C. Kuscu, J. Liu, and B.E. Bernstein performed ChIP and sequencing analysis. O. Abdel-Wahab, J. Gao, M. Adli, T. Trimarchi, T. Hricik, C. Kuscu, R. Koche, S. Li, X. Zhao, and C.E. Mason analyzed the data. O. Abdel-Wahab, J. Gao, I. Aifantis, and R.L. Levine prepared the manuscript with input from the other authors.

REFERENCES

Abdel-Wahab, O., M. Adli, L.M. LaFave, J. Gao, T. Hricik, A.H. Shih, S. Pandey, J.P. Patel, Y.R. Chung, R. Koche, et al. 2012. ASXL1 mutations promote myeloid transformation through loss of PRC2-mediated gene repression. *Cancer Cell*. 22:180–193. http://dx.doi.org/10.1016/j.ccr.2012.06.032

Bejar, R., K. Stevenson, O. Abdel-Wahab, N. Galili, B. Nilsson, G. Garcia-Manero, H. Kantarjian, A. Raza, R.L. Levine, D. Neuberg, and B.L. Ebert. 2011. Clinical effect of point mutations in myelodysplastic

JEM

syndromes. *N. Engl. J. Med.* 364:2496–2506. http://dx.doi.org/10.1056/NEJMoa1013343

Bejar, R., K.E. Stevenson, B.A. Caughey, O. Abdel-Wahab, D.P. Steensma, N. Galili, A. Raza, H. Kantarjian, R.L. Levine, D. Neuberg, et al. 2012. Validation of a prognostic model and the impact of mutations in patients with lower-risk myelodysplastic syndromes. *J. Clin. Oncol.* 30:3376–3382. http://dx.doi.org/10.1200/JCO.2011.40.7379

Boultwood, J., J. Perry, A. Pellagatti, M. Fernandez-Mercado, C. Fernandez-Santamaria, M.J. Calasanz, M.J. Larrayoz, M. Garcia-Delgado, A. Giagounidis, L. Malcovati, et al. 2010. Frequent mutation of the polycomb-associated gene ASXL1 in the myelodysplastic syndromes and in acute myeloid leukemia. *Leukemia.* 24:1062–1065. http://dx.doi.org/10.1038/leu.2010.20

Bracken, A.P., D. Kleine-Kohlbrecher, N. Dietrich, D. Pasini, G. Gargiulo, C. Beekman, K. Theilgaard-Mönch, S. Minucci, B.T. Porse, J.C. Marine, et al. 2007. The Polycomb group proteins bind throughout the INK4A-ARF locus and are disassociated in senescent cells. *Genes Dev.* 21:525–530. http://dx.doi.org/10.1101/gad.415507

Choi, C.W., Y.J. Chung, C. Slape, and P.D. Aplan. 2008. Impaired differentiation and apoptosis of hematopoietic precursors in a mouse model of myelodysplastic syndrome. *Haematologica.* 93:1394–1397. http://dx.doi.org/10.3324/haematol.13042

de Pontual, L., E. Yao, P. Callier, L. Faivre, V. Drouin, S. Cariou, A. Van Haeringen, D. Geneviève, A. Goldenberg, M. Oufadem, et al. 2011. Germline deletion of the miR-17~92 cluster causes skeletal and growth defects in humans. *Nat. Genet.* 43:1026–1030. http://dx.doi.org/10.1038/ng.915

Dey, A., D. Seshasayee, R. Noubade, D.M. French, J. Liu, M.S. Chaurushiya, D.S. Kirkpatrick, V.C. Pham, J.R. Lill, C.E. Bakalarski, et al. 2012. Loss of the tumor suppressor BAP1 causes myeloid transformation. *Science.* 337:1541–1546. http://dx.doi.org/10.1126/science.1221711

Fisher, C.L., I. Lee, S. Bloyer, S. Bozza, J. Chevalier, A. Dahl, C. Bodner, C.D. Helgason, J.L. Hess, R.K. Humphries, and H.W. Brock. 2010a. Additional sex combs-like 1 belongs to the enhancer of trithorax and polycomb group and genetically interacts with Cbx2 in mice. *Dev. Biol.* 337:9–15. http://dx.doi.org/10.1016/j.ydbio.2009.10.004

Fisher, C.L., N. Pineault, C. Brookes, C.D. Helgason, C. Ohta, C. Bodner, J.L. Hess, R.K. Humphries, and H.W. Brock. 2010b. Loss-of-function Additional sex combs like 1 mutations disrupt hematopoiesis but do not cause severe myelodysplasia or leukemia. *Blood.* 115:38–46. http://dx.doi.org/10.1182/blood-2009-07-230698

Gelsi-Boyer, V., V. Trouplin, J. Adélaïde, J. Bonansea, N. Cervera, N. Carbuccia, A. Lagarde, T. Prebet, M. Nezri, D. Sainty, et al. 2009. Mutations of polycomb-associated gene ASXL1 in myelodysplastic syndromes and chronic myelomonocytic leukaemia. *Br. J. Haematol.* 145:788–800. http://dx.doi.org/10.1111/j.1365-2141.2009.07697.x

Gilliland, D.G. 2001. The diverse role of the ETS family of transcription factors in cancer. *Clin. Cancer Res.* 7:451–453.

Haferlach, C., U. Bacher, S. Schnittger, T. Alpermann, M. Zenger, W. Kern, and T. Haferlach. 2012. ETV6 rearrangements are recurrent in myeloid malignancies and are frequently associated with other genetic events. *Genes Chromosomes Cancer.* 51:328–337. http://dx.doi.org/10.1002/gcc.21918

Hidalgo, I., A. Herrera-Merchan, J.M. Ligos, L. Carramolino, J. Nuñez, F. Martinez, O. Dominguez, M. Torres, and S. Gonzalez. 2012. Ezh1 is required for hematopoietic stem cell maintenance and prevents senescence-like cell cycle arrest. *Cell Stem Cell.* 11:649–662. http://dx.doi.org/10.1016/j.stem.2012.08.001

Hoischen, A., B.W. van Bon, B. Rodríguez-Santiago, C. Gilissen, L.E. Vissers, P. de Vries, I. Janssen, B. van Lier, R. Hastings, S.F. Smithson, et al. 2011. De novo nonsense mutations in ASXL1 cause Bohring-Opitz syndrome. *Nat. Genet.* 43:729–731. http://dx.doi.org/10.1038/ng.868

Itzykson, R., O. Kosmider, A. Renneville, V. Gelsi-Boyer, M. Meggendorfer, M. Morabito, C. Berthon, L. Adès, P. Fenaux, O. Beyne-Rauzy, et al. 2013. Prognostic score including gene mutations in chronic myelomonocytic leukemia. *J. Clin. Oncol.* 31:2428–2436. http://dx.doi.org/10.1200/JCO.2012.47.3314

Ivanova, N.B., J.T. Dimos, C. Schaniel, J.A. Hackney, K.A. Moore, and I.R. Lemischka. 2002. A stem cell molecular signature. *Science.* 298:601–604. http://dx.doi.org/10.1126/science.1073823

Jacobs, J.J., K. Kieboom, S. Marino, R.A. DePinho, and M. van Lohuizen. 1999. The oncogene and Polycomb-group gene bmi-1 regulates cell proliferation and senescence through the ink4a locus. *Nature.* 397:164–168. http://dx.doi.org/10.1038/16476

Jankowska, A.M., H. Makishima, R.V. Tiu, H. Szpurka, Y. Huang, F. Traina, V. Visconte, Y. Sugimoto, C. Prince, C. O'Keefe, et al. 2011. Mutational spectrum analysis of chronic myelomonocytic leukemia includes genes associated with epigenetic regulation: UTX, EZH2, and DNMT3A. *Blood.* 118:3932–3941. http://dx.doi.org/10.1182/blood-2010-10-311019

Klinakis, A., C. Lobry, O. Abdel-Wahab, P. Oh, H. Haeno, S. Buonamici, I. van De Walle, S. Cathelin, T. Trimarchi, E. Araldi, et al. 2011. A novel tumour-suppressor function for the Notch pathway in myeloid leukaemia. *Nature.* 473:230–233. http://dx.doi.org/10.1038/nature09999

Ko, M., H.S. Bandukwala, J. An, E.D. Lamperti, E.C. Thompson, R. Hastie, A. Tsangaratou, K. Rajewsky, S.B. Koralov, and A. Rao. 2011. Ten-Eleven-Translocation 2 (TET2) negatively regulates homeostasis and differentiation of hematopoietic stem cells in mice. *Proc. Natl. Acad. Sci. USA.* 108:14566–14571. http://dx.doi.org/10.1073/pnas.1112317108

Koschmieder, S., F. Rosenbauer, U. Steidl, B.M. Owens, and D.G. Tenen. 2005. Role of transcription factors C/EBPalpha and PU.1 in normal hematopoiesis and leukemia. *Int. J. Hematol.* 81:368–377. http://dx.doi.org/10.1532/IJH97.05051

Kühn, R., F. Schwenk, M. Aguet, and K. Rajewsky. 1995. Inducible gene targeting in mice. *Science.* 269:1427–1429. http://dx.doi.org/10.1126/science.7660125

Lakso, M., J.G. Pichel, J.R. Gorman, B. Sauer, Y. Okamoto, E. Lee, F.W. Alt, and H. Westphal. 1996. Efficient in vivo manipulation of mouse genomic sequences at the zygote stage. *Proc. Natl. Acad. Sci. USA.* 93:5860–5865. http://dx.doi.org/10.1073/pnas.93.12.5860

Li, Z., X. Cai, C.L. Cai, J. Wang, W. Zhang, B.E. Petersen, F.C. Yang, and M. Xu. 2011. Deletion of Tet2 in mice leads to dysregulated hematopoietic stem cells and subsequent development of myeloid malignancies. *Blood.* 118:4509–4518. http://dx.doi.org/10.1182/blood-2010-12-325241

Lin, Y.W., C. Slape, Z. Zhang, and P.D. Aplan. 2005. NUP98-HOXD13 transgenic mice develop a highly penetrant, severe myelodysplastic syndrome that progresses to acute leukemia. *Blood.* 106:287–295. http://dx.doi.org/10.1182/blood-2004-12-4794

Magini, P., M. Della Monica, M.L. Uzielli, P. Mongelli, G. Scarselli, E. Gambineri, G. Scarano, and M. Seri. 2012. Two novel patients with Bohring-Opitz syndrome caused by de novo ASXL1 mutations. *Am. J. Med. Genet. A.* 158A:917–921. http://dx.doi.org/10.1002/ajmg.a.35265

Metzeler, K.H., H. Becker, K. Maharry, M.D. Radmacher, J. Kohlschmidt, K. Mrózek, D. Nicolet, S.P. Whitman, Y.Z. Wu, S. Schwind, et al. 2011. ASXL1 mutations identify a high-risk subgroup of older patients with primary cytogenetically normal AML within the ELN Favorable genetic category. *Blood.* 118:6920–6929. http://dx.doi.org/10.1182/blood-2011-08-368225

Mizuki, M., J. Schwable, C. Steur, C. Choudhary, S. Agrawal, B. Sargin, B. Steffen, I. Matsumura, Y. Kanakura, F.D. Böhmer, et al. 2003. Suppression of myeloid transcription factors and induction of STAT response genes by AML-specific Flt3 mutations. *Blood.* 101:3164–3173. http://dx.doi.org/10.1182/blood-2002-06-1677

Moran-Crusio, K., L. Reavie, A. Shih, O. Abdel-Wahab, D. Ndiaye-Lobry, C. Lobry, M.E. Figueroa, A. Vasanthakumar, J. Patel, X. Zhao, et al. 2011. Tet2 loss leads to increased hematopoietic stem cell self-renewal and myeloid transformation. *Cancer Cell.* 20:11–24. http://dx.doi.org/10.1016/j.ccr.2011.06.001

Mueller, B.U., T. Pabst, M. Osato, N. Asou, L.M. Johansen, M.D. Minden, G. Behre, W. Hiddemann, Y. Ito, and D.G. Tenen. 2002. Heterozygous PU.1 mutations are associated with acute myeloid leukemia. *Blood.* 100:998–1007. http://dx.doi.org/10.1182/blood.V100.3.998

Mulligan, C.G., A. Kennedy, X. Zhou, I. Radtke, L.A. Phillips, S.A. Shurtleff, and J.R. Downing. 2007. Pediatric acute myeloid leukemia with NPM1 mutations is characterized by a gene expression profile with dysregulated HOX gene expression distinct from MLL-rearranged leukemias. *Leukemia.* 21:2000–2009. http://dx.doi.org/10.1038/sj.leu.2404808

Nilsson, L., I. Astrand-Grundström, I. Arvidsson, B. Jacobsson, E. Hellström-Lindberg, R. Hast, and S.E. Jacobsen. 2000. Isolation and characterization of hematopoietic progenitor/stem cells in 5q-deleted myelodysplastic

syndromes: evidence for involvement at the hematopoietic stem cell level. *Blood*. 96:2012–2021.

Nilsson, L., P. Edén, E. Olsson, R. Månsson, I. Astrand-Grundström, B. Strömbeck, K. Theilgaard-Mönch, K. Anderson, R. Hast, E. Hellström-Lindberg, et al. 2007. The molecular signature of MDS stem cells supports a stem-cell origin of 5q myelodysplastic syndromes. *Blood*. 110:3005–3014. http://dx.doi.org/10.1182/blood-2007-03-079368

Ohta, H., A. Sawada, J.Y. Kim, S. Tokimasa, S. Nishiguchi, R.K. Humphries, J. Hara, and Y. Takihara. 2002. Polycomb group gene rae28 is required for sustaining activity of hematopoietic stem cells. *J. Exp. Med*. 195:759–770. http://dx.doi.org/10.1084/jem.20011911

Pang, W.W., J.V. Pluvinage, E.A. Price, K. Sridhar, D.A. Arber, P.L. Greenberg, S.L. Schrier, C.Y. Park, and I.L. Weissman. 2013. Hematopoietic stem cell and progenitor cell mechanisms in myelodysplastic syndromes. *Proc. Natl. Acad. Sci. USA*. 110:3011–3016. http://dx.doi.org/10.1073/pnas.1222861110

Patel, J.P., M. Gönen, M.E. Figueroa, H. Fernandez, Z. Sun, J. Racevskis, P. Van Vlierberghe, I. Dolgalev, S. Thomas, O. Aminova, et al. 2012. Prognostic relevance of integrated genetic profiling in acute myeloid leukemia. *N. Engl. J. Med*. 366:1079–1089. http://dx.doi.org/10.1056/NEJMoa1112304

Quivoron, C., L. Couronné, V. Della Valle, C.K. Lopez, I. Plo, O. Wagner-Ballon, M. Do Cruzeiro, F. Delhommeau, B. Arnulf, M.H. Stern, et al. 2011. TET2 inactivation results in pleiotropic hematopoietic abnormalities in mouse and is a recurrent event during human lymphomagenesis. *Cancer Cell*. 20:25–38. http://dx.doi.org/10.1016/j.ccr.2011.06.003

Ramalho-Santos, M., S. Yoon, Y. Matsuzaki, R.C. Mulligan, and D.A. Melton. 2002. "Stemness": transcriptional profiling of embryonic and adult stem cells. *Science*. 298:597–600. http://dx.doi.org/10.1126/science.1072530

Raza-Egilmez, S.Z., S.N. Jani-Sait, M. Grossi, M.J. Higgins, T.B. Shows, and P.D. Aplan. 1998. NUP98-HOXD13 gene fusion in therapy-related acute myelogenous leukemia. *Cancer Res*. 58:4269–4273.

Rosenbauer, F., K. Wagner, J.L. Kutok, H. Iwasaki, M.M. Le Beau, Y. Okuno, K. Akashi, S. Fiering, and D.G. Tenen. 2004. Acute myeloid leukemia induced by graded reduction of a lineage-specific transcription factor, PU.1. *Nat. Genet*. 36:624–630. http://dx.doi.org/10.1038/ng1361

Ross, M.E., X. Zhou, G. Song, S.A. Shurtleff, K. Girtman, W.K. Williams, H.-C. Liu, R. Mahfouz, S.C. Raimondi, N. Lenny, et al. 2003. Classification of pediatric acute lymphoblastic leukemia by gene expression profiling. *Blood*. 102:2951–2959. http://dx.doi.org/10.1182/blood-2003-01-0338

Sanada, M., and S. Ogawa. 2012. Genome-wide analysis of myelodysplastic syndromes. *Curr. Pharm. Des*. 18:3163–3169. http://dx.doi.org/10.2174/1381612811209023163

Sawada, K., N. Sato, T. Tarumi, N. Sakai, K. Koizumi, S. Sakurama, M. Ieko, T. Yasukouchi, Y. Koyanagawa, M. Yamaguchi, et al. 1993. Proliferation and differentiation of myelodysplastic CD34+ cells in serum-free medium: response to individual colony-stimulating factors. *Br. J. Haematol*. 83:349–358. http://dx.doi.org/10.1111/j.1365-2141.1993.tb04656.x

Sawada, K., N. Sato, A. Notoya, T. Tarumi, S. Hirayama, H. Takano, K. Koizumi, T. Yasukouchi, M. Yamaguchi, and T. Koike. 1995. Proliferation and differentiation of myelodysplastic CD34+ cells: phenotypic subpopulations of marrow CD34+ cells. *Blood*. 85:194–202.

Shih, A.H., O. Abdel-Wahab, J.P. Patel, and R.L. Levine. 2012. The role of mutations in epigenetic regulators in myeloid malignancies. *Nat. Rev. Cancer*. 12:599–612. http://dx.doi.org/10.1038/nrc3343

Stadtfeld, M., and T. Graf. 2005. Assessing the role of hematopoietic plasticity for endothelial and hepatocyte development by non-invasive lineage tracing. *Development*. 132:203–213. http://dx.doi.org/10.1242/dev.01558

Steidl, U., F. Rosenbauer, R.G. Verhaak, X. Gu, A. Ebralidze, H.H. Otu, S. Klippel, C. Steidl, I. Bruns, D.B. Costa, et al. 2006. Essential role of Jun family transcription factors in PU.1 knockdown-induced leukemic stem cells. *Nat. Genet*. 38:1269–1277. http://dx.doi.org/10.1038/ng1898

Subramanian, A., P. Tamayo, V.K. Mootha, S. Mukherjee, B.L. Ebert, M.A. Gillette, A. Paulovich, S.L. Pomeroy, T.R. Golub, E.S. Lander, and J.P. Mesirov. 2005. Gene set enrichment analysis: a knowledge-based approach for interpreting genome-wide expression profiles. *Proc. Natl. Acad. Sci. USA*. 102:15545–15550. http://dx.doi.org/10.1073/pnas.0506580102

Tanaka, S., S. Miyagi, G. Sashida, T. Chiba, J. Yuan, M. Mochizuki-Kashio, Y. Suzuki, S. Sugano, C. Nakaseko, K. Yokote, et al. 2012. Ezh2 augments leukemogenicity by reinforcing differentiation blockage in acute myeloid leukemia. *Blood*. 120:1107–1117. http://dx.doi.org/10.1182/blood-2011-11-394932

Tehranchi, R., P.S. Woll, K. Anderson, N. Buza-Vidas, T. Mizukami, A.J. Mead, I. Astrand-Grundström, B. Strömbeck, A. Horvat, H. Ferry, et al. 2010. Persistent malignant stem cells in del(5q) myelodysplasia in remission. *N. Engl. J. Med*. 363:1025–1037. http://dx.doi.org/10.1056/NEJMoa0912228

Thol, F., I. Friesen, F. Damm, H. Yun, E.M. Weissinger, J. Krauter, K. Wagner, A. Chaturvedi, A. Sharma, M. Wichmann, et al. 2011. Prognostic significance of ASXL1 mutations in patients with myelodysplastic syndromes. *J. Clin. Oncol*. 29:2499–2506. http://dx.doi.org/10.1200/JCO.2010.33.4938

Vangala, R.K., M.S. Heiss-Neumann, J.S. Rangatia, S.M. Singh, C. Schoch, D.G. Tenen, W. Hiddemann, and G. Behre. 2003. The myeloid master regulator transcription factor PU.1 is inactivated by AML1-ETO in t(8;21) myeloid leukemia. *Blood*. 101:270–277. http://dx.doi.org/10.1182/blood-2002-04-1288

Vannucchi, A.M., T.L. Lasho, P. Guglielmelli, F. Biamonte, A. Pardanani, A. Pereira, C. Finke, J. Score, N. Gangat, C. Mannarelli, et al. 2013. Mutations and prognosis in primary myelofibrosis. *Leukemia*. 27:1861–1869. http://dx.doi.org/10.1038/leu.2013.119

Will, B., L. Zhou, T.O. Vogler, S. Ben-Neriah, C. Schinke, R. Tamari, Y. Yu, T.D. Bhagat, S. Bhattacharyya, L. Barreyro, et al. 2012. Stem and progenitor cells in myelodysplastic syndromes show aberrant stage-specific expansion and harbor genetic and epigenetic alterations. *Blood*. 120:2076–2086. http://dx.doi.org/10.1182/blood-2011-12-399683